

An X-ray census of young stars in the Chamaeleon I North cloudEric D. Feigelson^{1,2}

and

Warrick A. Lawson²**ABSTRACT**

Sensitive X-ray imaging surveys provide a new and effective tool to establish the census of pre-main sequence (PMS) stars in nearby young stellar clusters. We report here a deep *Chandra X-ray Observatory* observation of PMS stars in the Chamaeleon I North cloud, achieving a limiting luminosity of $\log L_t \simeq 27$ erg s^{-1} (0.5 – 8 keV band) in a 0.8×0.8 pc region. Of the 107 X-ray sources, 37 are associated with Galactic stars of which 27 are previously recognized cloud members. These include three PMS brown dwarfs; the protostellar brown dwarf ISO 192 has a particularly high level of magnetic activity. Followup optical photometry and spectroscopy establishes that 9-10 of the *Chandra* sources are probably magnetically active background stars. Several previously proposed cloud members are also inferred to be interlopers due to the absence of X-ray emission at the level expected from the $\log L_t - K$ correlation. No new X-ray discovered stars were confidently found despite the high sensitivity.

From these findings, we argue that the sample of 27 PMS cloud members in the *Chandra* field is uncontaminated and complete down to $K = 12$ or $M \simeq 0.1 M_{\odot}$. The initial mass function (IMF) derived from our sample is deficient in 0.1 – 0.3 M_{\odot} stars compared to the IMF of the rich Orion Nebula Cluster and other Galactic populations. We can not discriminate whether this is due to different star formation processes, mass segregation, or dynamical ejection of lower mass stars.

Subject headings: open clusters and associations: individual (Chamaeleon I) - stars:low-mass, brown dwarfs - stars: luminosity function, mass function - stars: pre-main sequence - X-rays: stars

¹Department of Astronomy & Astrophysics, Pennsylvania State University, University Park PA 16802

²School of Physical, Environmental & Mathematical Sciences, University of New South Wales, Australian Defence Force Academy, Canberra ACT 2600, Australia

1. Introduction

After many decades of study of the stellar initial mass function (IMF), recent progress has been made at defining the population of substellar objects (Kroupa 2002). Brown dwarfs (BDs) are much more luminous and have hotter surfaces shortly after birth compared to their later cooler stages as L and T dwarfs. It has thus proved possible to count them in young pre-main sequence (PMS) stellar clusters associated with nearby star formation region (e.g., Hillenbrand & Carpenter 2000; Muench et al. 2002; Briceño et al. 2002; Preibisch, Stanke, & Zinnecker 2003; Comerón 2003; Wilking et al. 2004). A strong suggestion has emerged that the very young BD population is lower in lower density star formation regions (like the Taurus-Auriga clouds) and higher density regions (like the Orion Nebula). Such studies are important for understanding the efficiency of gravitational collapse at low masses, the uniformity of the IMF under different cloud conditions, and the possible ejection of lower mass objects from multiple systems or circumstellar disks.

X-ray astronomical surveys of young stellar clusters has proved to be an effective complement to optical and near-infrared (O/NIR) surveys in defining PMS stellar populations. X-ray emission is elevated $10^1 - 10^4$ above old disk levels in virtually all stars 10^7 yrs and younger, providing an easy discriminant between PMS cluster members and most Galactic field stars (Feigelson & Montmerle 1999). X-rays trace magnetic activity, primarily magnetic reconnection flaring, which is relatively insensitive to the presence or absence of circumstellar disks. X-ray samples are thus particularly effective in recovering young stars where the disks have dissipated, often classified as weak-lined or post T Tauri stars. This relieves the bias towards diskless and accreting PMS stars that is often present in samples based on O/NIR surveys. An additional feature is a well-established empirical correlation between X-ray and photospheric brightness that links the X-ray luminosity function (XLF) with the K -band luminosity function (KLF). The astrophysical origin of this correlation is uncertain (Feigelson et al. 2003).

While previous generations of X-ray telescope had insufficient sensitivity and resolution to reveal the bulk of lower mass members of young stellar clusters, the *Chandra X-ray Observatory* can penetrate deeply into the PMS IMF. Intermediate-sensitivity *Chandra* studies had detected the majority of the stellar population and a modest fraction of the BD population in the ρ Ophiuchi, IC 348, σ Orionis and Orion Nebula young stellar clusters (Imanishi, Koyama, & Tsuboi 2001; Preibisch & Zinnecker 2002; Mokler & Stelzer 2002; Feigelson et al. 2002). X-ray studies thus join the active O/NIR efforts to identify and characterize future BDs that are contemporaneous with the PMS protostellar and T Tauri population.

We report here an unusually deep observation of the northern core of the Chamaeleon I

star forming cloud obtained with *Chandra*. Cha I was the site of the first X-ray discovered BD based on *ROSAT* imagery (Neuhauser & Comerón 1998) and a considerable number of candidate BDs have been reported using O/NIR photometric and spectroscopic techniques (Cambresy et al. 1998; Tamura et al. 1998; Oasa, Tamura, & Sugitani 1999; Comerón, Neuhauser & Kaas 2000; Gómez & Mardones 2003; López-Martí et al. 2004; Luhman 2004; Comerón et al. 2004(@)). Our *Chandra* observation is about 100 times more sensitive than the *ROSAT* observations due to a combination of lower detector background, wider bandwidth and longer exposure time. If the X-ray emission extends to substellar masses without change in the typical L_x/L_{bol} ratio, then we expect to detect many of the young BDs as well as the entire T Tauri population.

The Cha I cloud is particularly well-suited to studies of young stellar populations. First, it is one of the nearest active star formation regions at $d \simeq 160$ pc¹. Second, it is relatively isolated from other star forming clouds so there is little confusion due to older PMS stars that have drifted into the field. Third, the stellar population is relatively rich with a total population of 200 – 300 members. The population associated with the North cloud core has two additional advantages: the molecular material is confined to a small region so many members are only lightly obscured; and the stellar cluster is sufficiently compact that several dozen members can be studied in a single X-ray image. This molecular core, 296.5-15.7, has 30 M_⊙ of gas in a 0.4 pc (8′) diameter region with peak column density $\log N_H \simeq 22.3$ cm⁻² (Mizuno et al. 1999).

The stellar population of the Cha I North region has been surveyed at many spectral bands. The deepest of these surveys attain limits of $R \simeq 22$, $I \simeq 20$ (López-Martí et al. 2004), $J = 18.1$, $H = 17.0$, $K = 16.2$ (Oasa, Tamura, & Sugitani 1999), $L \simeq 11$ (Kenyon & Gómez 2001), $\simeq 2$ mJy in the 5 – 8.5 μm, $\simeq 4$ mJy in the 12 – 18 μm band (Persi et al. 2000), and $\simeq 150$ mJy at 1.3 mm (Reipurth, Nyman, & Chini 1996). It has also been examined for faint H α emitting stars (Hartigan 1993; López-Martí et al. 2004) and for X-ray emitting stars down to $\log L_x \simeq 29.0$ erg s⁻¹ in the soft *ROSAT* 0.3 – 2.4 keV band (Feigelson et al. 1993).

¹*Hipparcos* studies show that dust appears in the Chamaeleon region around 150 pc (Knude & Hog 1998) and the mean distance for seven stars in the cloud is 168(+14,-12) pc (Bertout, Robichon, & Arenou 1999). We adopt a distance of 160 pc.

2. *Chandra* observations and analysis

2.1. Data reduction and source detection

A $16' \times 16'$ region of the Cha I North cloud was observed with the imaging array of the Advanced CCD Imaging Spectrometer (ACIS-I) detector on board the *Chandra* X-ray Observatory. The satellite and instrument are described by Weisskopf et al. (2002). The detector aimpoint was set at $(\alpha, \delta) = (11^h 10^m 0.0^s, -76^\circ 35' 00'')$, epoch J2000. Figure 1 shows the field of view superposed on the molecular cloud; it subtends a 0.75×0.75 pc² region at the cloud. The observation took place on 2.25–3.04 July 2001 UT. With 1.3% of the exposure lost to CCD readout and 6 s lost to telemetry dropouts, the effective exposure was 66.3 ks.

The initial stages of data reduction are described in the Appendix of Townsley et al. (2003). Briefly, we start with the Level 1 events from the satellite telemetry, correct event energies for charge transfer inefficiency, and apply a variety of data selection operations such as ASCA event grades. Several bright sources near the field center with clear stellar counterparts in the 2MASS catalog (sources 41, 45, 48, 54, 57 and 62 in Table 1) were used to align the field to the *Hipparcos* reference frame. An offset of $0.15''$ was applied to the initial *Chandra* field position; the individual scatter of these alignment sources with respect to their 2MASS positions is $\pm 0.08''$.

Candidate sources were located using a wavelet-based detection algorithm (Freeman et al. 2002). We applied a low threshold ($P = 1 \times 10^{-5}$) so that some spurious sources are found which we exclude later. The image was visually examined for possible additional sources missed by the algorithm; no missing sources or close double sources were found. Events for each candidate source were extracted using the IDL- and CIAO-based script *acis_extract*². Here, events are extracted in a small region around each source containing 95% of the enclosed energy derived from the point spread function of the telescope at that position. A local background is defined from a nearby source-free region of each source and is scaled to the source extraction area.

Unreliable weak candidate sources are now removed. These include: sources with < 3.5 net (i.e. background-subtracted) extracted counts; faint sources with median energies above 5 keV that are probably fluctuations in the background; faint sources with poorly concentrated events; and faint sources with event arrival times indicating contamination by cosmic ray afterglows (i.e., several events appearing in a single pixel within 30 seconds). Near the field

²Description and code for *acis_extract* are available at http://www.astro.psu.edu/xray/docs/TARA/ae_users_guide.html.

center (off-axis angle $\theta < 5'$), source positions are simple centroids of the extracted events, while positions for sources far off-axis are obtained from a convolution of the point spread function with the extracted event positions. The *acis_extract* script also provides position-dependent telescope-plus-detector effective area *vs.* energy curves (*arf* files) and spectral resolution matrices (*rmf* files) for all sources.

The resulting 107 *Chandra* sources and shown in Figure 2 and their observed properties are given in Table 1. It gives the running source number, source position, off-axis angle, background-subtracted extracted counts (rounded to the nearest count), and cross-reference to the earlier *ROSAT* sources designated CHRX (Feigelson et al. 1993). Only 17 of the brightest sources were found with *ROSAT*³.

2.2. Stellar counterparts

Stellar counterparts are sought within $5''$ of the *Chandra* positions from five databases: the *JHK* band 2MASS all-sky catalog, the *IJK* band DENIS catalog, our *VI* band CCD images of the region (§3), the SIMBAD databases of published stars, and the list of Cha I cloud members collected from the literature by Carpenter et al. (2002). Twenty-seven previously known cloud members in Carpenter et al. (2002) were recovered in the *Chandra* observation, nearly all with positional offsets $< 0.5''$ as indicated in columns 7–8 of Table 1). Ten additional X-ray sources associated with previously unstudied stars are described in §5. We also discuss in §8.1 some published candidate cloud members lying in our *Chandra* field of view which are not X-ray detected. Figure 3 shows the stellar counterparts superposed on the dark cloud.

2.3. Stellar X-ray spectra and luminosities

Table 2 provide results from subsequent analysis of the X-ray properties of the stellar sources. The analysis used *acis_extract* version 1.1 for extraction and variability analysis, and XSPEC 11.2 for spectral modelling. C_x events were extracted in the polygon containing 95% of the full point spread function. B_x are the background counts scaled to the extraction

³The *ASCA* satellite, with low spatial resolution but a wide spectral band similar to *Chandra*'s, detected two sources in our ACIS field (Ueda et al. 2001): 1AXG J110943-7629 ($\log L_x = 30.4 \text{ erg s}^{-1}$) which blends our sources #38, 39, 40, 42 and possibly 41; and 1AXG J111011-7635 ($\log L_x = 30.8 \text{ erg s}^{-1}$) which blends #53, 56 and 61. These sources were earlier seen with the *Einstein* satellite with similar blending problems (Feigelson & Kriss 1989).

region.

The distribution of photon energies were modelled as emission from a thermal plasma with energy kT based on the emissivities calculated by Kaastra & Mewe (2000) subject to interstellar absorption. The absorption is expressed in equivalent hydrogen column densities, $\log N_H$ (cm^{-2}), assuming solar metallicities in the intervening gas. (Note, however, that the recent X-ray absorption study by Vuong et al. 2003 suggests that dark clouds have metallicities 20 – 30% lower than standard solar values.) Our modelling is limited by statistical considerations; weak sources (typically < 100 cts) are successfully modelled with 1-temperature plasmas, stronger sources (100 – 1000 cts) usually require 2-temperature plasmas, while the strongest sources (1000 – 3000 cts) often require 2- or 3-temperatures with non-solar elemental abundances. These flux-dependent differences are unphysical because magnetically active PMS stars, like the Sun, undoubtedly have continuous distributions of plasma emission measures over a wide range of temperatures. The fitted temperatures represent only the dominant plasma components of the star during the observation. The presence of non-solar abundances, particularly involving elements like iron and neon with extreme first ionization potentials, has been confirmed in high-resolution X-ray grating studies of stars with strong flare levels (Audard et al. 2003, and references therein). We thus caution that the spectral modeling does not reflect the full range of plasma properties and, for the fainter sources, may be nearly useless for interpreting plasma properties due to statistical uncertainties.

However, the broad-band luminosities integrated over the best-fit model are insensitive to spectral fitting uncertainties and have roughly $1/\sqrt{C_x}$ errors (Getman et al. 2002). The spectral model is used here as a nonlinear spline curve through the data. X-ray luminosities, L_s in the soft 0.5 – 2 keV band and L_t in the total 0.5 – 8 keV band, are obtained from these fluxes by multiplying by $4\pi d^2/0.95$ where $d = 160$ pc and 0.95 is the fraction of photons in the extraction region. These luminosities are from X-ray emission detected by the *Chandra* telescope and represent a lower limit to the emitted luminosities due to interstellar absorption. The absorption-corrected luminosities L_c are based on the best-fit spectral model assuming $\log N_H = 0$. The accuracy of these values is often low due to uncertainties in the fitting on nonlinear spectral models to the observed spectra. The L_c values should thus be used with caution.

2.4. X-ray variability

Column 5 of Table 2 gives a variability indicator based on the arrival times of the extracted events. It is coded to probability of the Kolmogorov-Smirnov test P_{KS} that the

source has no significant variation during the exposure: $a = P_{KS} > 0.05$ (no evidence for variability); $b = 0.005 > P_{KS} > 0.05$ (possibly variable); $c = P_{KS} < 0.005$ (definitely variable). Note that we expect several ‘b’ values but no ‘c’ values from a random collection of 107 constant sources. Lightcurves of prominent flares are shown in Figure 4.

3. Optical photometry and spectroscopy

The USNO-B1.0 catalog (Monet et al. 2003) provides *RI* photographic magnitudes and the 2MASS catalog provides *JHK* magnitudes for stellar counterparts across the ACIS field of view. There is also partial coverage of the field within the second release of the DENIS database at the *iJK* bands. To augment these surveys, we obtained *VI* band CCD images of most of the ACIS field with the 1-m telescope and CCD detector at the South African Astronomical Observatory (SAAO) during 2002 February. A $15' \times 15'$ field, centered near the *Chandra* aimpoint, was mapped with exposure times of 900s and 300s in the *V* and *I* bands, respectively. The SAAO survey covered the Cha I North core, but missed the extreme corners of the rotated ACIS field (Figure 2) where a number of counterparts are located. Comparison of source magnitudes obtained in the different surveys (SAAO *I* vs. DENIS *i* band magnitudes, and DENIS vs. 2MASS *JK* band magnitudes) indicate the various survey magnitudes can be freely interchanged, with discrepancies mostly comparable to the photometric errors. In Table 3 we list USNO-B1.0 *R*, DENIS *i* or SAAO *I*, and 2MASS *JHK* magnitudes for the stellar counterparts.

For three of the brighter candidates, we obtained 2 Å resolution spectroscopy in the region near H α and covering the Li I line at 6707.8 Å using the 2.3-m telescope and dual-beam spectrograph (DBS) at Siding Spring Observatory during 2003 April. In addition, 4 Å resolution spectra of six of the candidates were obtained for us by K. Luhman, using the Inamori Magellan Areal Camera and Spectrograph (IMACS) on the Magellan I telescope. We discuss the outcomes of our photometric and spectroscopic analysis of the new *Chandra* sources in §5.

4. Reliability and completeness of the stellar census

4.1. X-ray completeness limit

Our ability to detect sources in the ACIS field degrades with off-axis angle (due to broadening of the mirror point spread function) and with absorption (due to loss of soft X-ray photons). Feigelson et al. (2002, see their §2.12) develop formulae for such detection limits

taking into account technical factors such as optimal extraction radii, telescope vignetting and background subtraction. We adopt here a simpler approximation that fits the lower envelope of sources in Table 1. The limit in extracted counts as a function of off-axis angle θ (in arcmin) is then $C_{lim} \simeq 4$ cts for $\theta < 5'$ and $C_{lim} \simeq 4 + (\theta/5)^3$ cts for $5' < \theta < 11'$. The limiting luminosity in the total 0.5 – 8 keV band for a source with a typical PMS spectrum is then $\log L_{t,lim} \simeq 26.3 + \log C_{lim} + 0.3(\log N_H - 20.0)$ erg s⁻¹. Since cloud absorption is concentrated in the center of the ACIS field, it is doubtful that both C_{lim} and N_H are simultaneously high. For reasonable values of $C_{lim} \simeq 4 - 10$ cts and $\log N_H = 21 - 22$ cm⁻², the typical limiting sensitivity across the entire field is then $26.9 < \log L_{t,lim} < 27.5$ erg s⁻¹.

4.2. Stellar counterpart completeness

The O/NIR photometric surveys of Cha I North (§3) give counterpart information to limits of $R \approx 20$, $I \approx 18$, $J \approx 16$, and $H = K \approx 15$. At the distance to Cha I North ($d = 160$ pc) and adopting a maximum cloud absorption of $A_V \simeq 6 - 10$ magnitudes, these completeness limits exceed the Zero Age Main Sequence (ZAMS) for spectral types earlier than M5 ($M > 0.2 M_\odot$). For objects free from the regions of high extinction, the sub-stellar models of Baraffe et al. (1998) suggest that all cloud members with $M > 20 M_J$ and age $t < 10$ Myr (and still lower masses for younger ages) will appear as an O/NIR counterpart to any ACIS source.

Unlike earlier satellites where the poor resolution of proportional counters permitted multiple counterparts, *Chandra*'s excellent point spread function and satellite alignment give centroids accurate to a few tenths of an arcsecond on-axis. Counterpart ambiguities are thus restricted to multiple systems with component separations less than $\simeq 100$ AU.

The remaining challenge is then to distinguish stellar from the dominant extragalactic source population. This is facilitated by two tools. First, unresolved extragalactic counterparts of *Chandra* sources in our flux range are typically active galactic nuclei with redshifts $z < 3$ and faint magnitudes, $R \simeq 20 - 28$ (Hornschemeier et al. 2001; Barger et al. 2002). They rarely have $R < 19$. Second, extragalactic sources rarely vary on intra-day timescales. Of the 70 non-stellar sources in Table 1, 66 are consistent with constancy, 3 are possibly variable (consistent with a population of constant sources), and 1 is rapidly variable⁴. In

⁴This source #42 = CXO 110945.1-763022 has 17 events, 16 of which arrived in the final 14 ks of the exposure. Its spectrum is consistent either with a hot plasma ($kT > 3$ keV) or a powerlaw (photon index $\Gamma \sim 1$) subject to $\log N_H < 22.0$ cm⁻² absorption. This spectrum could emerge either from a star or an active galactic nucleus.

contrast, 11 of the 37 stellar sources are definitely variable and 6 are probably variable. Most of the remaining stellar sources have fewer than 100 photons so only the most dramatic variations can be seen.

Together, the optical magnitude and the X-ray variability distributions indicate that little if any erroneous confusion between extragalactic and stellar sources is present. The more subtle distinction between stars associated with the cloud and background field stars is discussed in §5 and §8.1.

5. New stellar counterparts to *Chandra* sources

We describe here the 10 ACIS sources coincident with O/NIR stars which have not previously been considered to be candidate members of the Cha I North star forming cloud. The relevant information are the photometric magnitudes and colors, our three Siding Spring Observatory and Magellan spectra (§3) and the X-ray properties. The magnitudes and colors alone prove to be a major constraint. Most of these stars are too faint to be PMS stars, or even ZAMS stars, at the distance of the cloud and do not have the very red colors associated with a low-luminosity young BD. They also lie in the outer regions of the ACIS field away from the core of the young stellar cluster. We conclude that they are mostly more distant stars unrelated to the cloud. In only one case where a strong emission line is present (# 16) is it feasible that the *Chandra*-discovered star may be a cloud member.

Qualitatively, it is not surprising that *Chandra* detects distant high-magnetic activity members of the Galactic field main sequence G, K and early-M population. Studies of solar neighborhood stars show that $\sim 10\%$ of K and early-M disk stars, and $\sim 30\%$ of G disk stars, have X-ray luminosities around $28.0 < \log L_x < 29.5 \text{ erg s}^{-1}$ (Schmitt, Fleming, & Giampapa 1995; Schmitt 1997). Such stars could be seen out to distances around 0.5 – 2 kpc in our ACIS exposure. A quantitative study of the background source contamination is complicated by absorption effects and stellar distributions in the Galactic disk; this lies beyond the scope of this investigation.

#16 This source lies $\sim 5'$ SW of the cloud core but suffers considerable soft X-ray absorption with moderate X-ray brightness. It has *JHK* colors consistent with a light-to-moderately reddened ($A_V \simeq 2 - 3$) early-M or late-K star without *K*-band excess. The IMACS spectrum confirms the late-K spectral type and detects $H\alpha$ in emission suggesting it is a young star. But the star is fainter than the ZAMS for its spectral type at the cloud distance of 160 pc, based on evolutionary models of Siess, Dufour, & Forestini (2000). If it is a cloud member, this might indicate the star is being seen in scattered light, although

thus usually occurs only in very heavily obscured PMS stars. While the preponderance of evidence points to a background star, we classify this as "Field?".q

#22 This source lies $\sim 6'$ north of the cloud core and is one of the weakest detected X-ray sources in the cloud. The *JHK* colors are consistent with a wide range of stellar types, from a weakly reddened M3 to a moderately ($A_V \simeq 5$) G star. But the star lies below the ZAMS for any of these possible spectral types. Showing strong interstellar Ca II absorption, the IMACS spectrum shows this is a background reddened G or K field star.

#24 This weak X-ray source lies $18''$ WNW of source #27 (= CHXR 79) which is $\simeq 40$ times brighter in the ACIS image. The ACIS spectrum is somewhat unusual, peaking around 1.3 keV and quickly dropping at both higher and lower energies probably indicating a high N_H column density. As with source #22, degeneracy in the *JHK* colors permit a spectral type between G and early-M, but require that it is a background star for any spectral type and extinction ($A_V \simeq 6 - 10$). IMACS spectroscopy also indicates a heavily reddened background star, although of uncertain spectral type.

#50 This weak source lies $\sim 8'$ N of the cloud core near the edge of the ACIS field. The ACIS spectrum appears moderately absorbed with best fit column density equivalent to $A_V \sim 5$, but statistical errors are consistent with the ambient cloud column density of $A_V \simeq 1 - 2$. The DBS and IMACS spectra indicate a weakly-reddened G star with strong Ca II absorption showing it must lie considerably beyond the cloud.

#79 This weak X-ray source appears about $7'$ NE of the cloud core. A brief flare may have occurred during the observation when 10 photons arrived within 1.5 hrs when only ~ 1 photon is expected from the remainder of the observation. The *JHK* colors are similar to star #22, and we thus believe it is another background field star.

#84 This weak source lies about $1'$ NE of the previous new X-ray star #79. The spectrum peaks at 1 keV and is consistent with no absorption, although moderate absorption up to a few magnitudes in A_V can not be excluded. The *JHK* colors suggest a B or A star with $A_V \simeq 3$, which is confirmed by DBS and IMACS spectroscopy. Its faintness requires a distance considerably further than the cloud. We note that BA stars themselves are not thought to be X-ray emitters due to the absence of an outer convective zone to generate and disrupt magnetic fields. X-ray emission from such stars is usually attributable to unseen late-type companions (Daniel, Linsky, & Gagné 2002; Stelzer et al. 2003).

#86 This source lies $8'$ SE of the cloud core and was detected only by virtue of a dramatic flare during the final 4 hours of the 19 hour observation (Figure 4j). The peak luminosity is $\log L_t \simeq \log L_c = 29.0 \text{ erg s}^{-1}$ and the quiescent luminosity is $< 27.3 \text{ erg s}^{-1}$ if the distance is 160 pc. The flare spectrum is very hard, exceeding *Chandra's* ability to

measure the temperature which we estimate to be $kT \geq 10$ keV. No soft energy absorption is evident. This is the only X-ray candidate source to show unequivocal high-amplitude flaring commonly seen in PMS stars.

The stellar counterpart to source #86 appears as a marginal detection on photographic sky surveys with $R \simeq 20.5$ and $I \simeq 18.4$. It is present at the sensitivity limits of the 2MASS J and H bands and is undetected in their K band. While source #86 is thus a candidate low luminosity cloud member, IMACS spectroscopy indicates a mid-M spectral type, and the distance modulus indicates it is probably a background flaring field star.

#88 This very faint ACIS source lies $\sim 7'$ W of the cloud core. The 2MASS JHK colors are unusual but are roughly consistent with a lightly reddened ($A_V \simeq 1$) M0 star. The star is too faint at this spectral type to be a cloud member and we thus classify it as a background field star.

#98 This very weak source lies $\sim 9'$ ENE of the cloud core in a region of low interstellar obscuration. The spectrum is soft with most of the events appearing below 1.2 keV. We note that such faint and soft sources will be missed in regions of higher interstellar absorption. The JHK colors suggest an unreddened G star and the faint magnitudes require location considerably beyond the cloud.

#99 This source lies $34''$ W of the weakly-reddened WTT star #103 = T 50 = Sz 40 about $10'$ E of the cloud core. It has ordinary X-ray properties with spectrum peaking at 1 keV and a low X-ray brightness. The DBS spectrum indicates a G star, consistent with JHK colors with no reddening. Here again, the star is too faint to lie at the cloud distance even if it were on the ZAMS.

6. Previously known Cha I North stars

Previously identified cloud members from Table 1 are briefly described here with a summary of their X-ray properties. Table 3 provides photometric, spectroscopic and inferred quantities (see table notes for details). Star designations and cross-identifications with various catalogs are obtained from Carpenter et al. (2002). Properties on these stars are obtained as follows: optical photometry and spectroscopy (Hartigan 1993; Huenemoerder, Lawson, & Feigelson 1994; Alcalá et al. 1995; Lawson, Feigelson, & Huenemoerder 1996; Saffe et al. 2003; López-Martí et al. 2004; Luhman 2004), pre-*Chandra* X-ray (Feigelson & Kriss 1989; Feigelson et al. 1993), near-IR photometry (Cambresy et al. 1998; Oasa, Tamura, & Sugitani 1999; Persi et al. 2000; Gómez & Kenyon 2001; Kenyon & Gómez 2001; Carpenter et al. 2002) and spectroscopy (Gómez & Persi 2002; Gómez & Mardones 2003). Both optical

and near-IR spectroscopy permit placement of stars on the HR diagram from which masses and ages can be inferred by comparison with PMS evolutionary tracks. As discrepancies in reported properties are often present, for consistency we give spectral types, bolometric luminosities, from the Magellan spectroscopic study of Luhman (2004), when available, with masses and ages inferred from Baraffe et al. (1998) evolutionary tracks. Note, however, that other studies often derive different inferred properties.

For convenience in this section, we use the phrasing: ‘light’, ‘moderate’ and ‘heavy’ absorption to refer to $A_V < 3$, $3 < A_V < 8$, and $A_V > 8$; ‘weak’, ‘moderate’ and ‘strong’ X-ray emission to refer to $\log L_c < 28.5$, $28.5 < \log L_c < 29.5$, and $\log L_c > 29.5$ erg s⁻¹; ‘high’, ‘intermediate’ and ‘low’ bolometric luminosity to refer to $\log L_{bol} \geq 1$, $0.1 < \log L_{bol} < 1$ L_⊙; and ‘very young’, ‘young’ and ‘older’ age to refer to $t \leq 1$, $1 < t < 5$, and $t > 5$ Myr. The nomenclature ‘WTT’ (weak-lined T Tauri) and ‘CTT’ (classical T Tauri) stars are used here loosely based on a combination of accretion and disk indicators.

#8 CHXR 33 = CHX 13a = C 1-10 = Cam1 65 = ISO 153 = KG 52 = ChaI 752 This is a moderately absorbed young M0 WTT star with intermediate L_{bol} and mass $M \simeq 0.7 M_{\odot}$. It has strong X-ray emission seen both with the *Einstein* and *ROSAT* satellites. The source exhibited a slow 30% increase over the 19 hour ACIS exposure which could easily arise from evolution in magnetically confined plasma or in the rotational modulation of coronal structures.

#15 T 37 = Sz 28 = Cam1 68 = ISO 157 = KG 54 = ChaI 709 This is a moderately absorbed CTT M5 star with strong H α but low L_{bol} indicating an older age. The X-ray emission is weak.

#25 CHXR 35 = Hn 8 = C 1-15 = Cam1 73 = KG 75 This is a lightly absorbed M5 $M \simeq 0.2 M_{\odot}$ CTT star with low L_{bol} and weak X-ray emission.

#26 CHXR 37 = Cam1 74 = ISO 185 = KG 77 = RX J1109.4-7627 This is a high- L_{bol} , moderately absorbed, very young K7 WTT star with $M \simeq 0.8 M_{\odot}$. The ACIS count distribution in the 0.9 – 1.3 keV spectral region can be successfully fit only with weak emission from the iron L-shell lines, implying a subsolar ([Fe/H] $\simeq 0.3$) abundance of iron in the heated plasma. This is commonly seen in the X-ray spectra of magnetically active stars. The X-ray luminosity is constant at $\log L_t \simeq 30$ erg s⁻¹. This combination of strong but constant emission is often attributed to heating by many microflares (Güdel et al. 2003).

#27 CHXR 79 = Hn 9 = C 1-18 = Cam1 75 = ISO 186 = KG 79 This is a heavily absorbed, young K7 CTT star with intermediate L_{bol} and $M \simeq 0.6 M_{\odot}$. A companion is present separated by 0.9" (Brandner et al. 1996). The X-ray emission is strong and constant.

#29 C 1-6 = Cam1 76 = ISO 189 = KG 82 = OTS 10 = ChaI 731 This is a very young, heavily absorbed, photometrically variable, M1 CTT star with intermediate L_{bol} and strong $H\alpha$. The moderate X-ray emission arises entirely from a flare during the first 3 hours of the exposure with peak $\log L_c \sim 29.6$ erg s⁻¹ (Figure 4a).

#33 ISO 192 = Cha I Northa2 = Cam2 41 = KG 87 = OTS 15 This star is an unusual outlier in $JHKL$ color-color diagrams with the strongest reddening ($A_V \sim 20$) and highest K - and L -band excess among Cha I members. This deeply embedded Class I protostar may be the driving source for the molecular bipolar flow at the center of the Cha I North cloud core (Persi et al. 1999). Together with its very low bolometric luminosity, these point to a protostar near or below the substellar boundary (Tamura et al. 1998). Mid-infrared spectroscopy shows strong absorption bands from silicates and ices characteristic of deeply embedded protostars (Pontoppidan et al. 2003; Alexander et al. 2003). Near-IR spectroscopy shows strong continuum veiling and strong molecular H₂ emission lines. After veiling correction, Gómez & Mardones (2003) derive a spectral type M6.5 with absorption $A_V \sim 22$, $L_{bol} \simeq 0.06 L_\odot$, $M \simeq 0.06 M_\odot$, and $t \simeq 0.4$ Myr. Perhaps most surprisingly, the K -band continuum has apparently brightened by over 2 magnitudes during the past several years (Pontoppidan et al. 2003).

The X-ray spectrum is heavily absorbed and, with less than 50 counts, unique spectral parameters can not be obtained. One satisfactory fit has a single $kT = 2$ keV plasma component with $\log N_H = 22.6$ cm⁻² ($A_V \sim 25$) giving an intrinsic absorption-corrected luminosity of $\log L_c \simeq 28.8$ erg s⁻¹. Other possibilities have absorption ranging up to $\log N_H \simeq 23$ cm⁻² ($A_V \sim 80$) with a strong soft plasma component and $\log L_c$ ranging up to $\simeq 30$ erg s⁻¹. The emission is not dominated by a high-amplitude flare. ISO 192 is thus a relatively strong X-ray emitter compared to most young BDs.

#38 CHXR 40 = Cam1 78 = ISO 198 = KG 92 This is a lightly absorbed, very young M1 WTT star with intermediate L_{bol} , $M \simeq 0.6 M_\odot$. It may be a wide binary with a faint 2MASS source 7'' to the south. The X-ray properties are similar to those of source #26: the emission is strong and constant, best fit with a reduced plasma iron abundance.

#41 C 1-25 = Cam1 79 = ISO 199 = KG 93 = OTS 19 C 1-25 is a heavily absorbed, photometrically variable star with a weak K-band photometric excess and no emission lines. Analysis of near-IR spectra give spectral type M1.5-2, $L_{bol} \simeq 1 L_\odot$, $M \simeq 0.2 M_\odot$ and $t < 0.1$ My. It is thus a very young, low mass WTT star with a remarkably strong X-ray flare. The X-ray light curve shows a dramatic flare rising steeply over the first 2 hours of observation, peaking at $\log L_c = 30.7$ erg s⁻¹, and then decaying over several hours with secondary flares to a quiescent level of $\log L_c = 29.7$ erg s⁻¹ (Figure 4b). The plasma temperature soared from 1 keV during the rise phase to > 10 keV at the peak, falling to ~ 5

keV during the decay phase and 2 keV at quiescence. The column density throughout was steady at $\log N_H = 22.2 \text{ cm}^{-2}$ ($A_V \simeq 10$).

#43 Hn 10E = T 42 = Sz 32 = C 1-24 = Cam1 82 = ISO 204 = KG 97 = OTS 24 This is an optically bright, moderately absorbed, very young M3 CTT star with intermediate L_{bol} and mass $M \simeq 0.2 M_\odot$ (Gómez & Mardones 2003). Its mid-IR spectrum shows unusually strong silicate emission around $10\mu\text{m}$ with no ice absorption features, possibly indicating a more evolved disk (Alexander et al. 2003). The X-ray luminosity is moderate with a relatively soft spectrum.

#44 T 41 = HD 97300 = CHXR 42 = C 1-11 = Cam1 85 = ISO 211 = KG 103 = OTS 26 = IRAS 11082-7620 HD 97300 illuminates the reflection nebula Ced 112 and is one of the highest mass members of the Cha I cloud. With spectral type B9V and mass $M \simeq 2 M_\odot$, it has been classified as a Herbig Ae/Be star without emission lines (The, de Winter, & Perez 1994). Its far-IR flux, presumably from a massive circumstellar disk, is very strong with an *IRAS* $60\mu\text{m}$ flux of 87 Jy. The primary has a lower mass companion with $\Delta K \simeq 3$ lying $0.74''$ to the NW (Ghez et al. 1997). At the beginning of our X-ray exposure, the emission rapidly (< 1 hr) dropped from $\log L_c \simeq 30.1 \text{ erg s}^{-1}$ to a quiescent level of $\log L_c \simeq 29.6 \text{ erg s}^{-1}$ which persisted for the remainder of the observation (Figure 4c). The flare peak luminosity could have been significantly higher.

The origin of X-ray emission from intermediate mass stars which have no outer convection zone has been the subject of long debate. The preponderance of evidence supports an origin in late-type companions (Feigelson et al. 2002; Stelzer et al. 2003). In the case of HD 97300, our X-ray position is accurate to $\pm 0.2''$ and agrees with the primary position to within $0.1''$, so it seems unlikely that the resolved companion with $0.7''$ offset is the X-ray source. We suggest that the X-rays arise from a yet-unresolved third component, although no evidence for spectroscopic binarity has been found in the primary (Corporon & Lagrange 1999).

#46 ISO 217 = KG 106 = GK 29 = ChaI 726 This is a low luminosity ($L_{bol} \simeq 0.03 L_\odot$) M6 star with estimated mass $M \simeq 0.07 M_\odot$, moderate absorption and a young age. It is thus a probable proto-brown dwarf. It also may be a visual binary. The X-ray source was only by virtue of a flare with $\log L_{peak} \simeq 29.0 \text{ erg s}^{-1}$; all but one of the 19 events arrived during the last 7 hours of the 18 hours observation (Figure 4d). The X-ray absorption suggests $A_V \simeq 30$, but this is poorly constrained by the few counts.

#47 T 42 = IRAS 11083-7618 = HM 23 = Sz 32 = C 1-5 = Cam1 86 = HBC 579 = ISO 223 = KG 109 = OTS 27 = ChaI 753 HM 23 is one of the more luminous CTT stars in the Cha I cloud with $L_{bol} = 3.5 L_\odot$. It has a K5 spectrum, estimated mass

of $1 M_{\odot}$, strong $H\alpha$ emission, heavy absorption and a massive disk emitting 50 Jy in the *IRAS* $60\mu\text{m}$ band. The X-ray emission is typically strong for PMS solar analogs (Feigelson, Garmire, & Pravdo 2002). A powerful flare with peak $L_t > 30.5 \text{ erg s}^{-1}$ began during the last 1/2 hour of the observation (Figure 4e).

#48 T 43 = Sz 33 = CHXR 41 = CHX 15 = C 1-17 = Cam1 87 = ISO 224 = KG 110 This is a young, moderately absorbed, photometrically variable M2 CTT star with an intermediate L_{bol} , $M \simeq 0.5 M_{\odot}$, and an infrared disk but relatively weak $H\alpha$ emission. The X-ray emission, seen earlier with the *Einstein* and *ROSAT* satellites, is strong. The luminosity decreased monotonically during the observation by 40%, plausibly due either to a slow decay of a flare or to rotational modulation of magnetic structures. The X-ray spectrum shows evidence for reduced iron and enhanced neon in the emitting plasma.

#49 ISO 225 = GK 31 This is a moderately absorbed, photometrically variable, very low luminosity ($L_{bol} \simeq 0.013 L_{\odot}$) CTT star in the cloud. The nature of this star has been difficult to unravel. The optical spectrum can be modelled as a M2 star from a $M \simeq 0.5 M_{\odot}$ star which is seen only in reflection (Luhman 2004), while the near-IR spectrum can be modelled as a M5 star with $M \simeq 0.1$ with strong continuum veiling and $A_V \simeq 5$ (Gómez & Mardones 2003). The X-ray luminosity of $\log L_t \simeq 29.0 \text{ erg s}^{-1}$ is consistent with any PMS star with $M \leq 0.5 M_{\odot}$ (Feigelson et al. 2003). The X-ray spectrum indicates an unusually hot plasma that is heavily absorbed equivalent to $A_V \simeq 30$, considerably higher than inferred from either the optical or infrared spectrum. The geometry of obscuring material around this star, which has the low luminosity of a proto-brown dwarf, may therefore be unusually complex.

#51 C 1-2 = Cam1 88 = ISO 226 = KG 111 = OTS 28 C 1-2 is a heavily absorbed CTT star invisible in the optical bands. The near-infrared spectrum indicates spectral type M1.5, heavy continuum veiling, $M \simeq 0.2 M_{\odot}$ and a very young age $< 0.1 \text{ Myr}$ (Gómez & Mardones 2003). The X-ray emission is heavily absorbed ($A_V \simeq 20$ with large uncertainty) and intermediate luminosity. Though statistically marginal, there may have been a flare lasting $\sim 6 \text{ hrs}$ during the middle of the observation.

#53 T 44 = WW Cha = HM 24 = Sz 34 = C 1-7 = HBC 580 = Cam1 90 = ISO 231 = KG 116 = OTS 29 = CHXR 44 WW Cha is a luminous, variable, rapidly rotating ($v \sin i = 56 \text{ km s}^{-1}$, Franchini et al. 1988), $M \simeq 0.8 - 1.0 M_{\odot}$, very young K5 CTT star with moderate absorption. It is one of the most luminous stars in the cloud with $L_{bol} \simeq 6 L_{\odot}$. The mid-IR spectrum shows unusually strong silicate emission around $10\mu\text{m}$ with no ice absorption features, possibly indicating a more evolved disk (Alexander et al. 2003). Its X-ray emission is very strong, exhibiting a short-lived ($< 1/2 \text{ hour}$) flare with a peak flux of $\log 30.6 \text{ erg s}^{-1}$ superposed on a high and more slowly variable emission

(Figure 4f).

#55 Hn 11 = C 1-4 = Cam1 91 = ISO 232 = KG 117 = OTS 35 Hn 11 is moderately absorbed, young CTT star with spectral type K8, intermediate L_{bol} and $M \simeq 0.75 M_{\odot}$. The X-ray emission is unremarkable with intermediate luminosity, absorption equivalent to $A_V \simeq 5$, and possible flaring.

#56 T 45a = HBC 582 = GK 1 = C 1-9 = HBC 582 = Cam1 92 = ISO 233 = KG 118 = IRAS 11085-7613 = CHXR 45 = CHX 16 GK 1 is a lightly absorbed, photometrically variable, $M \simeq 0.7 M_{\odot}$ M0 WTT star with strong X-ray emission seen earlier with the *Einstein* and *ROSAT* satellites. The X-ray luminosity is strong, and the lightcurve shows two short (0.5–2 hr) flares superposed on a high quiescent level (Figure 4g).

#58 T 46 = WY Cha = HM 26 = Sz 36 = C 1-16 = HBC 583 = Cam1 93 = ISO 234 = KG 119 = IRAS 11085-7613 = CHXR 46 WY Cha is a lightly absorbed, photometrically variable, young $M \simeq 0.8 M_{\odot}$ K8 CTT star with $L_{bol} \simeq 0.75 L_{\odot}$. The X-ray emission is strong. The lightcurve shows a flare with peak $\log L_t > 29.9 \text{ erg s}^{-1}$ superposed on a slower decline (Figure 4h).

#61 ISO 237 = C 1-8 = Cam2 48 = KG 121 = OTS 45 = ChaI 760 ISO 237 is a moderately absorbed, young K5 CTT star with estimated mass $M \simeq 0.9 M_{\odot}$ and luminosity $L_{bol} \simeq 1.3 L_{\odot}$. Its X-ray emission is moderately strong and constant.

#74 T 48 = WZ Cha = HM 28 = Sz 38 = C 1-23 = HBC 585 = Cam1 98 = ISO 258 = CHXR 82 WZ Cha is a lightly absorbed, variable, M1 CTT star with $M \simeq 0.7 M_{\odot}$, $L_{bol} \simeq 0.15 L_{\odot}$ and an unusually strong $H\alpha$ line. Due to its low luminosity, it has an old inferred age around $t \simeq 10 - 20 \text{ Myr}$. This appears to be a case where accretion has endured for many Myr. It has weak, soft and unabsorbed X-ray emission.

#75 Hn 13 = C 2-5 = Cam1 99 = ISO 259 = ChaI 755 This is a lightly absorbed, older M6 CTT star with $L_{bol} \simeq 0.16 L_{\odot}$, $M \simeq 0.08 M_{\odot}$ around the substellar limit. The X-ray spectrum implies heavier absorption around $A_V \simeq 20$ (with considerable uncertainty) which implies a strong intrinsic luminosity around $\log L_c \simeq 29.6 \text{ erg s}^{-1}$, far above the typical level for proto-brown dwarfs. The lightcurve shows a 6 hour flare-like variation (Figure 4i).

#91 CHXR 48 = E 1-7 = Cam1 101 = ISO 280 This is lightly absorbed, photometrically variable M2.5 WTT star with $L_{bol} = 0.25 L_{\odot}$ and $M \simeq 0.4 M_{\odot}$. It lies on the periphery of the cloud. The X-ray emission is strong and exhibited spectacular flaring with both rapid ($\simeq 1 \text{ hr}$) and slow ($> 6 \text{ hr}$) components with peak luminosity around

$\log L_t \simeq 30.5 \text{ erg s}^{-1}$ (Figure 4k). The X-ray spectrum implies sub-solar iron abundance in the plasma, as commonly found in flaring stars.

#100 CHXR 84 = Hn 16 = Cam1 105 = E 1-10 = ChaI 742 This is a lightly absorbed M5.5 cloud member lying off the cloud core with estimated mass $M \simeq 0.1 M_\odot$ and $L_{bol} \simeq 0.12 L_\odot$. With only one measurement of H α with 20 Å equivalent width and no *K*-band excess, it probably should be classified as a WTT star. The X-ray emission is moderate with a spectral evidence for a reduced iron abundance.

#103 T 50 = Sz 40 = E 1-5 = HBC 587 = Cam1 106 = CHXR 85 = ChaI 757 This is a very young, photometrically variable M5 CTT star with $M \simeq 0.1 M_\odot$ and $L_{bol} \simeq 0.19 L_\odot$. The optical spectrum indicates light absorption of $A_V \simeq 1$ and it lies in an unobscured region off the cloud core, but the strong X-ray emission has an unusual spectrum best fit by a soft plasma suffering heavy absorption equivalent to $A_V \simeq 12$ (with considerable uncertainty). But with only 60 counts for analysis, this finding can not be considered definitive.

#105 T 51 = Sz 41 = HBC 588 = E 1-9a = Cam1 107 = IRAS 11108-7620 = CHX 20b = CHXR 50 This is a visually very bright, unabsorbed, older K3.5 WTT star off the cloud core with $L_{bol} \simeq 1.1 L_\odot$ and $M \simeq 1.2 M_\odot$. It is a visual binary with a fainter companion 1.5'' to the south-east; the similarly bright star $\simeq 12''$ to the east is not a cloud member (Ghez et al. 1997; Walter 1992). It has no *K*-band excess but nonetheless appears to have a faint outer disk seen with *IRAS*. The star appears relatively faint during the *Chandra* observation with only 50 counts and $\log L_t \simeq 29.0 \text{ erg s}^{-1}$; this is an order of magnitude fainter than during the earlier *ROSAT* pointed, *ROSAT* All-Sky Survey, and *Einstein* observations. However, the source is at the edge of the ACIS detector and, due to the broad off-axis PSF, many photons are probably lost during satellite dithering.

7. Relationships between X-rays and other properties of PMS stars

Despite many years of empirical investigation, some fundamental uncertainties remain in our understanding of the astrophysical origins of X-ray emission of PMS stars. It is clear that the X-rays are produced by plasma magnetically confined and heated to $10^7 - 10^8 \text{ K}$. Violent magnetic reconnection events similar to, but more powerful than, contemporary solar flares are often seen in the X-ray lightcurves. But there has been debate regarding the geometry of the reconnecting magnetic fields: solar-type fields rooted in the stellar surface; long field lines connecting the star to the corotation radius of the disk; or fields entirely associated with the disk (Feigelson & Montmerle 1999). It is further puzzling that X-ray luminosities show

strong correlation with the closely intertwined properties of stellar bolometric luminosity, size and mass and is not closely linked to stellar rotation as seen in main sequence stars (Feigelson et al. 2003; Flaccomio, Micela, & Sciortino 2003). Soft X-ray absorption can also be compared with optical-infrared reddening to constraint the gas-to-dust ratio of cloud. We consider these issues only briefly here because the Cha I North population is small and our findings are not novel. Stellar properties are presented in Table 3; for consistency, most values are adopted from Luhman (2004).

Figure 5a shows a broad correlation extending over 2 – 3 orders of magnitude between X-ray luminosity and K -band magnitude⁵. The $L_x - L_{bol}$ correlation, commonly seen in PMS populations, looks very similar to this plot. The similar rough correlation between $\log L_t$ and mass M (Figure 5b) is expected from the link between mass and L_{bol} in a roughly coeval PMS population. A weak anti-correlation between $\log L_t$ and age may be present (Figure 5c), but this may be an indirect effect of the below-average bolometric luminosities and masses of the few older stars in the field.

The outlier with high L_{bol} and M but only average L_t is HD 97300. The low L_t/L_{bol} ratio of intermediate-mass B and A PMS stars is often seen in PMS populations, and is usually attributed to X-ray production by an unresolved magnetically active low-mass companion rather than the more massive star which does not have an outer convection zone (e.g. Feigelson et al. 2002; Stelzer et al. 2003).

Past studies have discussed whether or not the X-ray luminosities of non-accreting WTT stars are systematically elevated compared to accreting CTT stars (Preibisch & Zinnecker 2002; Flaccomio, Micela, & Sciortino 2003, and references therein). The issue is important for interpreting the astrophysical origin of PMS X-ray emission but is complicated by sample biases and the $\log L_t - \log L_{bol}$ correlation. Adopting the classifications given in column 4 of Table 3 and the intrinsic absorption-corrected 0.5 – 8 keV luminosities $\log L_c$, we find mean values of $\langle \log L_c \rangle = 29.8 \pm 0.2 \text{ erg s}^{-1}$ for 10 cataloged WTT stars and $\langle \log L_c \rangle = 29.3 \pm 0.2 \text{ erg s}^{-1}$ for 16 cataloged CTT stars. As our sample is likely complete $M \geq 0.1 M_\odot$ (§8), the reported excess of WTT over CTT X-ray emission appears to be confirmed. However, we see no systematic differences between CTTs and WTT stars in the bivariate $\log L_x - K$ diagrams or in X-ray variability or spectral. Our results are thus not conclusive on this issue.

⁵In this panel, the *Chandra* sources identified as field stars are plotted as open circles under the probably-incorrect assumption they lie at $d = 160 \text{ pc}$. They are included here to emphasize that the limiting sensitivity of the *Chandra* observation lies considerably below the weakest confirmed cloud members, which is important for evaluation of the sample completeness (§8).

The N_H column densities obtained from X-ray spectral fitting represent a measurement of the total (i.e. solid, molecular, atomic and ionized) intervening interstellar gas which can be compared to the independent optical/IR measurement of reddening by dust alone (Vuong et al. 2003). The six most heavily absorbed stars with > 100 ACIS counts – CHXR 79, C 1-25, T 42, T 43, T 44, and ISO 237 ($A_V \simeq 7$) – have $5 < A_V < 16$. Together these stars give an interstellar absorption ratio $N_H/A_V \simeq 1 \times 10^{21} \text{ cm}^{-2}/\text{mag}$, lower than the traditional value of $2 \times 10^{21} \text{ cm}^{-2}/\text{mag}$. This difference is in the same direction as the more reliable and well-substantiated value $N_H/A_V = 1.6 \times 10^{21} \text{ cm}^{-2}/\text{mag}$ derived by Vuong et al. (2003) from a larger sample of heavily absorbed PMS stars in the ρ Ophiuchus cloud.

8. Discussion: The cloud population

As outlined in §1, X-ray surveys provide a method to obtain the census of a PMS stellar cluster with different selection effects and different sources of contamination than encountered in O/NIR surveys. The value of Cha I North is its proximity, compactness, and unusually intensive study at O/NIR wavelengths (Cambresy et al. 1998; Oasa, Tamura, & Sugitani 1999; Comerón, Neuhauser & Kaas 2000; Gómez & Mardones 2003; López-Martí et al. 2004; Luhman 2004; Comerón et al. 2004(@)). We combine these with our *Chandra* observation giving an very sensitive X-ray survey down to $\log L_x \simeq 27 \text{ erg s}^{-1}$ to give new insight into the cloud population and its initial mass function.

8.1. A complete sample of 27 cloud members

We have already argued that our X-ray source list is complete to $\log L_t \simeq 26.9 - 27.5 \text{ erg s}^{-1}$ where the value depends on the individual stars' absorption and location in the ACIS field (§4.1). This is more sensitive than almost all previously published studies of young stellar populations which generally have limiting $\log L_t \geq 28.0 \text{ erg s}^{-1}$. Of the 107 ACIS sources (Table 1), 69 are confidently classified as extragalactic and 37 are confidently classified as stellar (§4.2). The remaining ambiguous source (#42) shows rapid variability resembling a PMS star but has no O/NIR counterpart. Of the 37 stellar X-ray sources, 9 are classified as non-PMS background stars (§5). One additional X-ray source (#16) has a stellar counterpart that is probably a magnetically active field star. but could be a cloud member seen with an unusual geometry.

The remaining 27 ACIS sources discussed in §6 constitute the X-ray selected sample of cloud members. This sample has no known contaminants and (except for the possible

additions of #16 and #42) is complete in X-ray luminosity. There are no anomalies where a confident bright O/NIR member is undetected in X-rays. Based on the correlations between L_t , L_{bol} and M (§7), we now argue that this sample is also complete to interesting limits in bolometric luminosity and mass. Recalling that the O/NIR surveys of the region are not limited by sensitivity (they can detect all objects with $M > 20 M_J$ with $t < 10$ Myr (§4.2), the issue here is the evaluation of non-cloud contaminants in various O/NIR samples.

Figure 6 compares the $\log L_t - K$ relationship for the 27 Cha I North stars (previously seen in Figure 5a) with that seen in the more populous Orion Nebula Cluster⁶. The Chamaeleon I and Orion samples clearly occupy the same region in the diagram and show the same correlation. The shaded band indicates our Cha I North X-ray completeness limit (§4.1).

We use the Orion sample in Figure 6 to argue that, at a distance of 160 pc, an X-ray survey complete to $\log L_t \simeq 26.9 - 27.5$ erg s⁻¹ is also complete to $K \simeq 11$ and will capture the majority of stars with $11 < K < 12$. We are confident of this conclusion even without knowing the exact nature of the $\log L_t - K$ relation and its scatter at low luminosities because no cloud members were found below $\log L_t = 28.2$ erg s⁻¹. We consider this to be important: the ACIS image should have detected all cloud members between $26.9 - 27.5 < \log L_t < 28.2$ erg s⁻¹. Half of the extragalactic sources and most of the field star sources (open circles in Figure 5a) were found at these low flux levels, so there clearly is no operational difficulty in detecting such sources. The exception would be cloud members with extremely high absorption, $\log N_H > 23$ cm⁻² or $A_V > 100$, such as the Class 0 protostar Cha-MMS 2 (Reipurth, Nyman, & Chini 1996). With this caveat, we conclude that the X-ray complete sample of 27 cloud members represents a complete and uncontaminated census of cloud members with $K \leq 12$ lying in the ACIS field.

One byproduct of this result is a clarification of the membership status of several O/NIR stars discussed in the literature. Six stars – ISO 154, ISO 164, ISO 165, Ced112 IRS2, ISO 247 (Carpenter et al. 2002) and ESO-H α 564 (Comerón et al. 2004(@)) – have $10.2 < K < 11.7$ and are undetected in the ACIS image. These can be excluded from cloud membership with

⁶The Orion sample is obtained from the tables of the *Chandra* Orion Ultradeep Project (COUP) provided by Getman et al. (2004). The sample here consists of 399 COUP sources with counterparts in the *JHKL* catalog of Muench et al. (2002). The Orion K magnitudes have been artificially increased by 2.0 to place them at a distance of 160 pc rather than 450 pc. $\log L_t$ values were obtained using *ACIS Extract* package consistent with our analysis here. This Orion sample should not be viewed as complete (in particular, there are additional COUP sources with fainter K -band counterparts; M. McCaughrean, private communication), but rather gives a larger PMS population to better define the correlation and scatter in the $\log L_t - K$ diagram.

considerable confidence⁷. Most of these X-ray-quiet stars have independently been evaluated to be background stars based on optical spectra by Luhman (2004). The exception is the M5.5 star ISO 165, a slightly reddened \sim M5 star with strong H α but negligible infrared excess (Kenyon & Gómez 2001; López-Martí et al. 2004), which Luhman classifies as a cloud member but which we believe is a non-member due to the X-ray non-detection. With only one such disagreement, we find a gratifying agreement between our X-ray and Luhman’s spectroscopic census of cloud members considering that the selections are based on very different criteria.

8.2. The KLF and IMF

Having established that our sample of 27 stars is largely complete and uncontaminated to $K \simeq 12$, we readily construct the K -band luminosity based on K magnitudes in Table 3. Figure 7a compares compares our Cha I North KLF to that of the Orion Nebula Cluster derived by Muench et al. (2002) after scaling (as in Figure 6) by $\Delta K = 2.0$ to account for the difference in distance. We see that both KLFs show a similar rise from bright magnitudes to a peak around $K \simeq 9.5$. The fall off at faint magnitudes appears somewhat steeper in Cha I North, but the difference is not statistically significant.

Figure 7b shows the Cha I North IMF for our sample using masses given in Table 3, and compares it to both the IMF inferred for the ONC (Hillenbrand & Carpenter 2000) and a general Galactic IMF derived by Kroupa (2001) from a variety of cluster and field star populations. Here, a deficiency of lower mass stars in Cha I North is clearly present. The Cha I North IMF peaks in the $0.3 - 1.0 M_{\odot}$ bin while the other IMFs peak around $0.1 M_{\odot}$. The effect is statistically significant. A Kolmogorov-Smirnov two-sample test between the ONC and Chamaeleon I North IMFs indicate only a 0.3% probability (3σ equivalent) they are drawn from the same population. Alternatively, if one considers the ratio of stars in the $(0.1-0.3):(0.3-1.0) M_{\odot}$ bins, the observed ratio in Cha I North of 5:14 has a 99% confidence ratio $0.09 - 0.72$ while the Orion and Kroupa IMFs predict a ratio around 1.5. The difference can be erased only if a considerable number of Cha I North stars are present that simultaneously have K below our completeness limit $\simeq 12$ and masses above $M \simeq 0.1 M_{\odot}$; i.e., an older PMS population superposed on the younger well-characterized population.

We thus establish a deficit of $0.1 - 0.3 M_{\odot}$ stars in Cha I North compared to standard IMFs We can tentatively and qualitatively extend this inference to the BD regime. Three

⁷The X-ray measurement do not clarify the membership status of C 1-14, a reddened F0 star with $K = 7.8$ because F stars often have soft coronal X-ray spectra which could be fully absorbed by interstellar gas.

previously known objects at or below the stellar limit are detected: ISO 192, ISO 217 and Hn 13. But no additional X-ray selected population (with the possible exception of the rapidly variable source #42 with no reported O/NIR counterpart) is seen. If a large number of BDs were present, we would expect a fraction of them to have X-ray luminosities above our sensitivity and appear in the ACIS image. This result is consistent with reports of poor BD populations in the Taurus-Auriga and IC 348 star forming regions (Luhman 2000; Briceño et al. 2002; Preibisch, Stanke, & Zinnecker 2003). However, this argument can not be made quantitatively until the COUP survey establishes the scatter about the $L_t - L_{bol}$ and $L_t - K$ relationships in substellar PMS objects.

It may be that the Cha I North cloud has an intrinsically non-standard IMF due to its star formation process. For example, the population of lowest mass stars may be sensitive to the spectrum of the turbulent velocity field in the cloud (Delgado-Donate, Clarke, & Bate 2004). But, it is critical to recall that the deficiency of lower mass stars applies only to the $16' \times 16'$ (0.8×0.8 pc) ACIS field. We thus can not exclude alternative hypotheses that place the lower mass stars preferentially outside the ACIS field of view. It seems plausible that mass segregation is present leading to a surfeit of higher mass stars in the cloud core. This could either be a characteristic of the primordial cluster formation process or a later dynamical development. Evidence for primordial mass segregation has been found both in the rich Orion Nebula Cluster (Bonnell & Davies 1998) and in the sparse η Cha cluster (Lyo et al. 2004). Dynamical segregation could also occur if lower mass stars are preferentially born with a velocity dispersion greater than the higher mass stars, or if they are ejected from multiple systems due to close gravitational encounters (e.g. Reipurth & Clarke 2001; Kroupa & Bouvier 2003b). A velocity dispersion difference as small as ≥ 0.2 km s⁻¹ is sufficient for stars to travel outside the ACIS field in $\simeq 2$ Myr, a typical age of the Cha I North stars.

9. Conclusions

The low-mass population of the Chamaeleon I cloud has been investigated in the O/NIR bands by several groups but with discrepant samples and differing conclusions (Cambresy et al. 1998; Persi et al. 2000; Comerón, Neuhauser & Kaas 2000; Gómez & Mardones 2003; López-Martí et al. 2004; Luhman 2004). Some are optimistic that a significant population of low mass stars and substellar objects are being found within the heavily contaminated infrared samples, while others suggest BDs are deficient or that the census is too incomplete to reach clear conclusions. We bring to bear here a distinct and complementary method for identifying PMS stars of all masses: high sensitivity, high resolution imagery with the *Chandra* X-ray Observatory. Our *Chandra* survey with limiting $\log L_t \simeq 27$ erg s⁻¹, suffi-

cient to detect the contemporary active Sun, should be complete to $K \simeq 12$ or $M \geq 0.1 M_{\odot}$. Equally importantly, X-ray surveys of this type can confidently tell when an O/NIR star is *not* a cloud member because of the enormous difference in L_x/L_{bol} ratios for PMS and old disk stars which frequently contaminate O/NIR surveys.

We find no cloud members with $26.9 - 27.5 < \log L_t < 28.3$ erg s⁻¹ (0.5 – 8 keV band), and no more than one new X-ray discovered cloud member is present. We furthermore confirm that several previously suspected cloud members are probably background stars. The result is a nearly complete and uncontaminated sample of 27 cloud members in the ACIS field of the Cha I North cloud. The IMF of this sample is significantly deficient in 0.1 – 0.3 M_{\odot} stars compared to the IMF of the rich Orion Nebula Cluster and of the general stellar IMF. This supports recent observational studies that report deficits in the BD population in low density star formation regions (Briceño et al. 2002; Preibisch, Stanke, & Zinnecker 2003). However, our X-ray field of view is rather small, so we can not discriminate between a true deficiency in low mass stars and alternative explanations such as mass segregation or dynamical ejection of the lowest mass PMS stars⁸.

From the forthcoming COUP study, we are likely to learn how the relationships between L_t and L_{bol} , K and M extend into the substellar regime. This will permit us to derive quantitative inferences regarding the BD population in Cha I North. At the present time, we can say only qualitatively that this population appears to be small as we would expect some fraction to have X-ray luminosities exceeding $\log L_t \simeq 27$ erg s⁻¹. Three of the 27 stars in our complete sample – ISO 192, ISO 217 and (probably) Hn 13 – lie below the substellar limit and, by virtue of their X-ray emission, are confirmed cloud members.

The reliability of the X-ray census method used here rests on the empirical relationships between L_t and K and the closely related correlations between L_t , L_{bol} and masses M among PMS stars. These relationships have been seen in nearly all well-studied PMS stellar clusters with *Chandra*: the ONC (Flaccomio, Micela, & Sciortino 2003; Feigelson et al. 2003), NGC 1333 (Getman et al. 2002), IC 348 (Preibisch & Zinnecker 2002), Mon R2 (Kohnno, Koyama, & Hamaguchi 2002) and NGC 2024 (Skinner, Gagné, & Belzer 2003). Given their importance, it is worrisome that these relationships between magnetic activity and bulk stellar properties are largely unexplained (Feigelson et al. 2003). But if one accepts them, these relationships permit a translation between an observational X-ray flux limit and limits in the KLF and

⁸As this study goes to press, Stelzer et al. (2004) announced results from an *XMM – Newton* X-ray study of the Cha I South region. Their image is larger but several times less sensitive than our *Chandra* ACIS image. They detect two bona fide brown dwarfs and several H α emitting objects near the hydrogen burning mass limit. It is possible that Cha I South does not share the same IMF as the inner region of Cha I North we study here.

IMF. Our confidence in the reliability and completeness of X-ray surveys will increase as we improve our characterization of these relationships and scatter about them.

Finally, we bring to attention one remarkable low mass PMS star. ISO 192 was already known to have the heaviest absorption and strongest NIR color excess among Cha I members with heavy spectroscopic veiling and large photometric variability. It has been interpreted as a substellar ($\sim 60 M_J$) Class I protostar and the likely source of the Cha I North molecular bipolar flow. We add here another unusual characteristic: strong magnetic activity with intrinsic X-ray luminosity around 10^{29} erg s $^{-1}$.

Acknowledgements Kevin Luhman (CfA) generously shared results from unpublished Magellan spectra, A-Ran Lyo (UNSW@ADFA) assisted with the optical spectroscopy, and Lisa Crause (UCT) helped with the optical photometry. We thank the SAAO and MSSSO Telescope Allocation Committees for observing time, and EDF appreciates the University of New South Wales and Australian Defence Force Academy for hospitality during much of this work. We greatly benefitted from the SIMBAD and USNO databases, and made use of data products from the Two Micron All Sky Survey which is a joint project of the University of Massachusetts and the Infrared Processing and Analysis Center/California Institute of Technology funded by NASA and the NSF. This study was principally supported by NASA's *Chandra* Guest Observer program grant GO1-2005 (EDF,PI) and UNSW@ADFA URSP, FRG and SRG research grants (WAL, PI).

REFERENCES

- Alcala, J. M., Krautter, J., Schmitt, J. H. M. M., Covino, E., Wichmann, R., & Mundt, R. 1995, *A&AS*, 114, 109
- Alexander, R. D., Casali, M. M., André, P., Persi, P., & Eiroa, C. 2003, *A&A*, 401, 613
- Audard, M., Güdel, M., Sres, A., Raassen, A. J. J., & Mewe, R. 2003, *A&A*, 398, 1137
- Baraffe, I., Chabrier, G., Allard, F., & Hauschildt, P. H. 1998, *A&A*, 337, 403
- Barger, A. J., Cowie, L. L., Brandt, W. N., Capak, P., Garmire, G. P., Hornschemeier, A. E., Steffen, A. T., & Wehner, E. H. 2002, *AJ*, 124, 1839
- Bertout, C., Robichon, N., & Arenou, F. 1999, *A&A*, 352, 574
- Bonnell, I. A. & Davies, M. B. 1998, *MNRAS*, 295, 691
- Brandner, W., Alcala, J. M., Kunkel, M., Moneti, A., & Zinnecker, H. 1996, *A&A*, 307, 121
- Briceño, C., Luhman, K. L., Hartmann, L., Stauffer, J. R., & Kirkpatrick, J. D. 2002, *ApJ*, 580, 317
- Brinkman, A. C. et al. 2001, *A&A*, 365, L324
- Cambresy, L., Epchtein, N., Copet, E., de Batz, B., Kimeswenger, S., Le Bertre, T., Rouan, D., & Tiphene, D. 1997, *A&A*, 324, L5
- Cambresy, L., Copet, E., Epchtein, N., de Batz, B., Borsenberger, J., Fouque, P., Kimeswenger, S., & Tiphene, D. 1998, *A&A*, 338, 977
- Carpenter, J. M., Hillenbrand, L. A., Skrutskie, M. F., & Meyer, M. R. 2002, *AJ*, 124, 1001
- Comerón, F., Neuhauser, R. & Kaas, A. A. 2000, *A&A*, 359, 269
- Comerón, F. 2003, in *Brown Dwarfs* (E. Martín, ed.), IAU Symp. 211, San Francisco:ASP, 5
- Comerón, F. & Claes, P. 2004, *ApJ*, 602, 298
- Comeronón, F., Reipurth, B., Henry, A. & Fernánde, M. 2004, preprint
- Corporon, P. & Lagrange, A.-M. 1999, *A&AS*, 136, 429
- Daniel, K. J., Linsky, J. L., & Gagné, M. 2002, *ApJ*, 578, 486
- Delgado-Donate, E. J., Clarke, C. J., & Bate, M. R. 2004, *MNRAS*, 347, 759

- Feigelson, E. D. & Kriss, G. A. 1989, *ApJ*, 338, 262
- Feigelson, E. D. & Montmerle, T., *ARA&A*, 37, 363
- Feigelson, E. D., Casanova, S., Montmerle, T., & Guibert, J. 1993, *ApJ*, 416, 623
- Feigelson, E. D., Broos, P., Gaffney, J. A., Garmire, G., Hillenbrand, L. A., Pravdo, S. H., Townsley, L., & Tsuboi, Y. 2002, *ApJ*, 574, 258
- Feigelson, E. D., Garmire, G. P., & Pravdo, S. H. 2002, *ApJ*, 572, 335
- Feigelson, E. D., Gaffney, J. A., Garmire, G., Hillenbrand, L. A., & Townsley, L. 2003, *ApJ*, 584, 911
- Flaccomio, E., Micela, G., & Sciortino, S. 2003, *A&A*, 397, 611
- Franchini, M., Stalio, R., & Magazzu, A. 1988, *A&A*, 189, 132
- Freeman, P. E., Kashyap, V., Rosner, R., & Lamb, D. Q. 2002, *ApJS*, 138, 185
- Getman, K. V., Feigelson, E. D., Townsley, L., Bally, J., Lada, C. J., & Reipurth, B. 2002, *ApJ*, 575, 354
- Getman, K. V., et al. 2004, to be submitted
- Ghez, A. M., McCarthy, D. W., Patience, J. L., & Beck, T. L. 1997, *ApJ*, 481, 378
- Gómez, M. & Kenyon, S. J. 2001, *AJ*, 121, 974
- Gómez, M. & Persi, P. 2002, *A&A*, 389, 494
- Gómez, M. & Mardones, D. 2003, *AJ*, 125, 2134
- Güdel, M., Audard, M., Kashyap, V. L., Drake, J. J., & Guinan, E. F. 2003, *ApJ*, 582, 423
- Hartigan, P. 1993, *AJ*, 105, 1511
- Hillenbrand, L. A. & Carpenter, J. M. 2000, *ApJ*, 540, 236
- Hornschemeier, A. E. et al. 2001, *ApJ*, 554, 742
- Huenemoerder, D. P., Lawson, W. A., & Feigelson, E. D. 1994, *MNRAS*, 271, 967
- Imanishi, K., Koyama, K., & Tsuboi, Y. 2001, *ApJ*, 557, 747

- Kaastra, J. S. & Mewe, R. 2000, in *Atomic Data Needs for X-ray Astronomy*, NASA/CP-2000-209968, 161
- Kenyon, S. J. & Gómez, M. 2001, *AJ*, 121, 2673
- Knude, J. & Hog, E. 1998, *A&A*, 338, 897
- Kohno, M., Koyama, K., & Hamaguchi, K. 2002, *ApJ*, 567, 423
- Kroupa, P. 2001, *MNRAS*, 322, 231
- Kroupa, P. 2002, *Science*, 295, 82
- Kroupa, P. & Bouvier, J. 2003, *MNRAS*, 346, 34
- Kroupa, P. & Bouvier, J. 2003, *MNRAS*, 346, 369
- Lawson, W. A., Feigelson, E. D., & Huenemoerder, D. P. 1996, *MNRAS*, 280, 1071
- López-Martí, B., Eislöffel, J., Scholz, A. & Mundt, R. 2004, *A&A*, 416, 555
- Lyo, A.-R., Lawson, W. A., Feigelson, E. D., & Crause, L. A. 2004, *MNRAS*, 347, 246
- Luhman, K. L. 2000, *ApJ*, 544, 1044
- Luhman, K. L., 2004, *ApJ*, 602, 816
- Mizuno, A. et al. 1999, *PASJ*, 51, 859
- Mokler, F. & Stelzer, B. 2002, *A&A*, 391, 1025
- Monet, D. G., et al. 2003, *AJ*, 125, 984
- Muench, A. A., Lada, E. A., Lada, C. J., & Alves, J. 2002, *ApJ*, 573, 366
- Neuhauser, R. & Comerón, F. 1998, *Science*, 282, 83
- Oasa, Y., Tamura, M., & Sugitani, K. 1999, *ApJ*, 526, 336
- Persi, P., Marenzi, A. R., Kaas, A. A., Olofsson, G., Nordh, L., & Roth, M. 1999, *AJ*, 117, 439
- Persi, P. et al. 2000, *A&A*, 357, 219
- Pontoppidan, K. M., Dartois, E., van Dishoeck, E. F., Thi, W.-F., & d'Hendecourt, L. 2003, *A&A*, 404, L1

- Preibisch, T. & Zinnecker, H. 2002, *AJ*, 123, 1613
- Preibisch, T., Stanke, T., & Zinnecker, H. 2003, *A&A*, 409, 147
- Reipurth, B., Nyman, L.-A., & Chini, R. 1996, *A&A*, 314, 258
- Reipurth, B. & Clarke, C. 2001, *AJ*, 122, 432
- Saffe, C., Randich, S., Mardones, D., Caselli, P., Persi, P., & Racca, G. 2003, *A&A*, 409, 993
- Schmitt, J. H. M. M., Fleming, T. A., & Giampapa, M. S. 1995, *ApJ*, 450, 392
- Schmitt, J. H. M. M. 1997, *A&A*, 318, 215
- Siess, L., Dufour, E., & Forestini, M. 2000, *A&A*, 358, 593
- Skinner, S., Gagné, M., & Belzer, E. 2003, *ApJ*, 598, 375
- Stelzer, B., Huélamo, N., Hubrig, S., Zinnecker, H., & Micela, G. 2003, *A&A*, 407, 1067
- Stelzer, B., Micela, G., & Neuhäuser, R. 2004, *A&A*, in press
- Tamura, M., Itoh, Y., Oasa, Y., & Nakajima, T. 1998, *Science*, 282, 1095
- The, P. S., de Winter, D., & Perez, M. R. 1994, *A&AS*, 104, 315
- Townsley, L. et al. 2003, *ApJ*, in press
- Ueda, Y., Ishisaki, Y., Takahashi, T., Makishima, K., & Ohashi, T. 2001, *ApJS*, 133, 1
- Vuong, M. H., Montmerle, T., Grosso, N., Feigelson, E. D., Verstraete, L. & Ozawa, H., 2003, *A&A*, in press
- Walter, F. M. 1992, *AJ*, 104, 758
- Weisskopf, M. C., Brinkman, B., Canizares, C., Garmire, G., Murray, S., & Van Speybroeck, L. P. 2002, *PASP*, 114, 1
- Wilking, B. A., Meyer, M. R., Greene, T. P., Mikhail, A., & Carlson, G. 2004, *AJ*, 127, 1131

Table 1. *Chandra* sources and counterparts in Cha I North

#	X-ray source					Stellar counterpart	
	R.A.	Dec.	θ	Cts	CHRX	Star	Δ
(1)	(2)	(3)	(4)	(5)	(6)	(7)	(8)
1	11 07 13.6	-76 38 55.2	10.9	12
2	11 07 34.4	-76 34 33.9	8.9	30
3	11 07 45.1	-76 35 32.3	8.3	37
4	11 08 10.2	-76 29 01.8	8.8	15
5	11 08 18.9	-76 32 54.9	6.7	13
6	11 08 21.2	-76 33 51.6	6.3	19
7	11 08 23.9	-76 33 07.8	6.3	4
8	11 08 40.8	-76 36 07.8	5.3	990	33	CHXR 33	0.4
9	11 08 41.5	-76 34 51.0	5.0	49
10	11 08 42.8	-76 36 36.8	5.3	33
11	11 08 44.3	-76 34 38.2	4.9	22
12	11 08 46.0	-76 26 23.9	9.5	12
13	11 08 48.3	-76 40 55.4	7.8	10
14	11 08 50.9	-76 38 00.1	5.6	6
15	11 08 50.9	-76 25 14.5	10.4	42	...	T 37	1.0
16	11 08 51.4	-76 38 26.3	5.8	54	...	Field?	0.2
17	11 08 56.6	-76 33 41.2	4.3	7
18	11 09 01.2	-76 33 56.9	4.0	17
19	11 09 01.3	-76 34 17.0	3.9	34
20	11 09 05.3	-76 23 51.4	11.4	31
21	11 09 07.4	-76 32 16.2	4.3	14
22	11 09 10.6	-76 27 12.5	8.2	8	...	Field	2.1
23	11 09 11.8	-76 31 37.0	4.5	8
24	11 09 13.5	-76 30 23.7	5.3	23	...	Field	0.6
25	11 09 13.9	-76 28 40.0	6.8	158	35	CHXR 35	0.5
26	11 09 17.8	-76 27 58.2	7.3	2348	37	CHXR 37	0.5
27	11 09 18.3	-76 30 29.5	5.1	843	79	CHXR 79	0.5
28	11 09 22.3	-76 39 03.0	5.1	6
29	11 09 22.6	-76 34 32.0	2.6	26	...	C 1-6	0.4
30	11 09 22.7	-76 28 48.7	6.4	16
31	11 09 27.2	-76 41 38.7	7.4	22

Table 1—Continued

#	X-ray source					Stellar counterpart	
	R.A.	Dec.	θ	Cts	CHRX	Star	Δ
(1)	(2)	(3)	(4)	(5)	(6)	(7)	(8)
32	11 09 27.3	-76 34 30.1	2.4	9
33	11 09 28.5	-76 33 28.2	2.6	46	...	ISO 192	0.1
34	11 09 31.1	-76 29 01.7	6.1	16
35	11 09 31.5	-76 28 22.1	6.7	16
36	11 09 33.3	-76 32 52.3	2.7	6
37	11 09 38.4	-76 38 47.5	4.5	10
38	11 09 40.1	-76 28 39.5	6.2	2846	40	CHXR 40	0.5
39	11 09 40.9	-76 29 46.5	5.1	33
40	11 09 41.6	-76 30 42.2	4.3	7
41	11 09 41.9	-76 34 58.5	1.5	2328	...	C 1-25	0.1
42	11 09 45.1	-76 30 22.2	4.5	16
43	11 09 46.2	-76 34 46.4	1.3	75	...	Hn 10E	0.1
44	11 09 50.1	-76 36 47.6	2.4	1105	42	T 41	0.1
45	11 09 51.1	-76 27 15.3	7.5	42
46	11 09 52.1	-76 39 12.9	4.6	17	...	ISO 217	0.3
47	11 09 53.4	-76 34 25.6	0.9	699	...	T 42	0.1
48	11 09 54.1	-76 29 25.4	5.3	1189	41	T 43	0.1
49	11 09 54.4	-76 31 11.6	3.6	60	...	ISO 225	0.4
50	11 09 54.8	-76 25 35.0	9.1	17	...	Field	1.8
51	11 09 55.0	-76 32 40.9	2.1	37	...	C 1-2	0.1
52	11 09 56.6	-76 27 35.7	7.1	21
53	11 10 00.1	-76 34 57.9	0.5	2516	44	T 44	0.1
54	11 10 00.7	-76 43 29.2	8.8	25
55	11 10 03.7	-76 33 29.3	1.2	62	...	Hn 11	0.2
56	11 10 04.7	-76 35 45.2	1.1	2055	45	T 45a	0.0
57	11 10 06.3	-76 29 48.4	4.9	73
58	11 10 07.0	-76 29 37.9	5.1	1781	46	T 46	0.3
59	11 10 07.9	-76 34 23.3	0.3	63
60	11 10 09.4	-76 41 48.7	7.2	16
61	11 10 11.4	-76 35 29.2	0.8	331	...	ISO 237	0.0
62	11 10 12.1	-76 37 26.7	2.8	11

Table 1—Continued

#	X-ray source					Stellar counterpart	
	R.A.	Dec.	θ	Cts	CHRX	Star	Δ
(1)	(2)	(3)	(4)	(5)	(6)	(7)	(8)
63	11 10 13.8	-76 37 39.0	3.0	6
64	11 10 22.4	-76 27 16.1	7.5	143
65	11 10 27.5	-76 27 19.3	7.5	79
66	11 10 32.1	-76 41 09.5	6.6	8
67	11 10 36.2	-76 34 10.3	1.7	19
68	11 10 36.9	-76 31 32.6	3.6	42
69	11 10 41.3	-76 34 09.9	2.0	4
70	11 10 46.8	-76 45 14.7	10.9	46
71	11 10 47.2	-76 30 44.2	4.6	7
72	11 10 52.5	-76 29 16.3	6.0	59
73	11 10 52.6	-76 28 09.8	7.0	438	80
74	11 10 53.3	-76 34 31.9	2.6	73	82	T 48	0.0
75	11 10 55.9	-76 45 32.8	11.2	106	...	Hn 13	0.4
76	11 10 58.3	-76 40 03.9	6.1	13
77	11 11 01.8	-76 32 36.4	3.7	12
78	11 11 04.0	-76 39 03.2	5.4	12
79	11 11 05.1	-76 29 41.4	6.0	19	...	Field	0.4
80	11 11 06.4	-76 32 39.8	3.9	90
81	11 11 09.8	-76 37 13.0	4.4	15
82	11 11 10.1	-76 36 27.0	4.0	7
83	11 11 10.6	-76 32 33.1	4.2	4
84	11 11 16.9	-76 28 57.9	7.0	12	...	Field	0.7
85	11 11 19.7	-76 34 49.0	4.2	17
86	11 11 20.0	-76 38 25.7	5.6	40	...	Field	0.8
87	11 11 21.6	-76 35 12.0	4.3	5
88	11 11 23.6	-76 33 55.1	4.4	7	...	Field	2.0
89	11 11 24.2	-76 37 43.1	5.4	322	83
90	11 11 25.9	-76 36 06.2	4.7	70
91	11 11 34.7	-76 36 21.2	5.3	1768	48	CHXR 48	0.2
92	11 11 38.5	-76 30 40.2	6.6	37
93	11 11 40.8	-76 38 59.9	6.9	17

Table 1—Continued

#	X-ray source					Stellar counterpart	
	R.A.	Dec.	θ	Cts	CHRX	Star	Δ
(1)	(2)	(3)	(4)	(5)	(6)	(7)	(8)
94	11 11 41.3	-76 36 39.0	5.7	8
95	11 11 44.9	-76 40 16.8	7.9	24
96	11 11 47.2	-76 29 33.1	7.7	10
97	11 11 49.1	-76 30 29.8	7.2	158
98	11 12 00.1	-76 31 28.2	7.3	10	...	Field	0.2
99	11 12 00.2	-76 34 30.0	6.5	21	...	Field	0.4
100	11 12 03.2	-76 37 03.3	7.1	113	84	CHXR 84	0.3
101	11 12 04.5	-76 33 43.2	6.8	60
102	11 12 05.4	-76 31 37.6	7.5	235
103	11 12 09.7	-76 34 35.4	7.1	60	85	T 50	1.3
104	11 12 19.6	-76 31 43.8	8.2	63
105 ^a	11 12 23.2	-76 37 04.3	8.2	50	50	T 51	4.8
106	11 12 26.3	-76 35 30.2	8.1	14
107	11 12 46.9	-76 32 04.2	9.6	27

Note. — Table columns:

1. Running number for this paper.

2-3. Position from the ACIS image aligned to 2MASS sources. Generally, positions are accurate to $< 0.3''$ for off-axis angle $\theta < 5'$ and $Cts > 100$. Positional accuracy degrades to $\sim 1''$ for fainter on-axis sources, and to $2-3''$ for sources far off-axis ($\theta > 10'$).

4. Off-axis angle in arcmin.

5. Cts are the 0.5 – 8 keV events in the 95% enclosed-energy polygon after subtraction of background and rounded to the nearest integer obtained from *acis_extract*.

6. CHXR is the *ROSAT* source number from Feigelson et al. (1993).

7. Name from the cloud membership list by Carpenter et al. (2002). ‘Field’ indicates previously unremarked stellar counterparts. The remainder of the X-ray sources are probably extragalactic.

8. Offset in arcsec between the Chandra and 2MASS positions.

^aSource #105 lies at the edge of the ACIS detector where, due to the broad telescope point spread function and satellite dithering, many of the source photons may be lost. This can result in an underestimate of the source luminosity and an apparent positional offset of the centroid.

Table 2. X-ray properties of *Chandra* Cha I North stellar sources

#	Name	C_x	B_x	Var	$\log N_H$	kT_1	kT_2	$\log L_s$	$\log L_t$	$\log L_c$
(1)	(2)	(3)	(4)	(5)	(6)	(7)	(8)	(9)	(10)	(11)
8	CHXR 33	993	3	c	21.8	0.7±0.3	...	29.3	29.4	30.0
15	T 37	68	24	a	0	2.0±1.3	...	27.9	28.1	28.1
16	Field?	57	3	a	22.1	1.3±0.4	...	27.9	28.3	28.7
22	Field	15	7	a	0:	2:	...	27.1	27.4	27.4
24	Field	25	2	a	22.3	0.3	...	27.4	27.4	...
25	CHXR 35	164	6	a	21.8	0.2	1.0	28.6	28.6	30.1
26	CHXR 37	2357	9	a	21.7	0.4	2.2	29.6	29.8	30.4
27	CHXR 79	845	2	a	21.8	0.6±0.1	...	28.9	29.7	29.8
29	C 1-6	27	1	c	22.4	2.2±1.3	...	27.3	28.3	28.8
33	ISO 192	47	1	a	23:	2:	...	27.1	28.6	^a
38	CHXR 40	2853	7	a	0	0.8	2.5	29.8	29.9	29.9
41	C 1-25	2329	1	c	22.2	10:	...	29.2	30.3	30.4
43	Hn 10E	76	1	a	22.0	0.9±0.2	...	28.1	28.2	28.9
44	T 41	1106	1	c	21.3	0.8	3.2	29.2	29.5	29.7
46	ISO 217	17	2	c	22.4	5:	...	27.1	28.3	28.5
47	T 42	699	0	b	21.8	0.7	4.9	29.2	29.7	30.0
48	T 43	1192	3	c	21.8	0.4	2.5	29.6	29.6	30.1
49	ISO 225	61	1	b	22.7	10:	...	26.8	28.9	29.1
50	Field	25	8	a	21.9	1.3±2.1	...	27.5	27.8	28.3
51	C 1-2	38	1	b	22.4	3.2±2.1	...	27.4	28.5	28.8
53	T 44	2517	1	c	21.8	0.6	2.8	29.8	30.2	30.5
55	Hn 11	63	1	b	21.9	2.1±0.8	...	27.9	28.4	28.7
56	T 45a	2056	1	b	21.6	0.8	2.4	29.5	29.8	30.1
58	T 46	1784	3	c	21.1	0.6	2.4	29.6	29.7	29.8
61	ISO 237	332	1	a	22.0	0.7	4.2	28.8	29.2	29.7
74	T 48	74	1	a	0	0.8±0.2	...	28.2	28.4	28.4
75	Hn 13	130	24	c	22.4	1.4±0.4	...	28.0	28.8	29.6
79	Field	23	4	b	21:	0.5±0.6	...	27.6	27.6	28.6
84	Field	18	6	a	0	1.1±0.4	...	27.3	27.3	27.3
86	Field	44	4	c	0	10:	...	27.8	28.3	28.3
88	Field	8	1	a	0	1:	...	27.1	27.2	27.2
91	CHXR 48	1771	3	c	21.4	0.4	1.7	29.6	29.7	30.0

Table 2—Continued

#	Name	C_x	B_x	Var	$\log N_H$	kT_1	kT_2	$\log L_s$	$\log L_t$	$\log L_c$
(1)	(2)	(3)	(4)	(5)	(6)	(7)	(8)	(9)	(10)	(11)
98	Field	15	5	a	0	0.8 ± 0.2	...	27.6	27.6	27.6
99	Field	25	4	a	0	2.1 ± 1.1	...	27.6	27.8	27.8
100	CHXR 84	119	6	a	0	1.0 ± 0.1	...	28.4	28.5	28.5
103	T 50	65	5	a	22.3	0.9 ± 0.4	...	28.0	28.3	29.4
105 ^b	T 51	53	3	a	21.8	0.8 ± 0.2	...	28.6	28.7	29.3

Note. — The X-ray luminosities assume the star lies at a distance of 160 pc. The Field stars discussed in §5 lie on the far side of the cloud at unknown distances, so their X-ray luminosities are greater than the tabulated values.

^aSee text, §6.

^bSee note to Table 1.

Table 3. Optical-infrared properties of *Chandra* Cha I North stellar sources

#	Star	Prop Flag	Class	Photometry							HR Diagram			
				R	i/I	J	H	K	m(6.7)	m(14.3)	SpTy	L_{bol}	Mass	Age
(1)	(2)	(3)	(4)	(5)	(6)	(7)	(8)	(9)	(10)	(11)	(12)	(13)	(14)	(15)
8	CHXR 33	0YYY00	WTT	14.5	12.59	10.56	9.66	9.28	8.73	...	M0	0.42	0.7	3
15	T 37	0Y00Y0	CTT	...	14.60	12.45	11.73	11.30	10.1	...	M5.25	0.04?	0.1	8
16	Field?	17.4	16.39	14.58	13.63	13.33
22	Field	17.0	16.13	14.65	13.86	13.51
24	Field	19.6	17.88	15.01	13.64	13.05
25	CHXR 35	0Y0Y00	CTT	16.1	13.91	11.85	11.21	10.87	M4.75	0.072	0.2	3
26	CHXR 37	0YYY00	WTT	13.2	11.72	10.00	9.04	8.70	8.47	8.3	K7	1.0	0.8	1
27	CHXR 79	YY0YY0	CTT	16.8	14.99	11.66	10.12	9.07	7.12	5.55	M1.25	0.47	0.6	2
29	C 1-6	Y000Y0	CTT	19.5	16.79	12.60	10.35	8.67	5.84	3.73	M1.25	0.77	0.6	1
33	ISO 192	Y000Y0	I/BD	16.07	13.27	11.04	6.40	2.83
38	CHXR 40	0YYY00	WTT	12.9	11.66	10.07	9.23	8.96	8.73	...	M1.25	0.69	0.6	1
41	C 1-25	Y000Y0	WTT	13.80	11.42	10.00	7.05	4.91
43	Hn 10E	0Y00YY	CTT	16.7	14.70	11.95	10.74	10.05	7.7	5.8	M3.25	0.18	0.25	3
44	T 41	000YYY	AB/WTT	8.8	8.82	7.64	7.35	7.35	2.84	0.93	B9	61.	2.7	1
46	ISO 217	0000Y0	BD?	19.4	16.63	13.53	12.54	11.82	9.8	...	M6.25	0.028	0.07	3
47	T 42	YY00YY	CTT	17.0	11.79	9.47	7.79	6.46	3.58	1.57	K5	3.5	1.0:	<1
48	T 43	YY0YY0	CTT	15.8	14.03	11.30	10.00	9.25	7.66	5.91	M2	0.46	0.55	3
49	ISO 225	Y000Y0	CTT	18.4	17.23	15.05	13.80	13.14	9.3	7.6	M1.75	0.013	0.5:	...
50	Field	15.4	14.70	13.60	12.95	12.71
51	C 1-2	Y000YY	CTT	...	17.85	13.78	11.30	9.67	6.34	4.34
53	T 44	YY0YY0	CTT	12.6	10.95	8.71	7.21	6.08	3.62	1.64	K5	6.1	1.0:	<1
55	Hn 11	0Y00Y0	CTT	15.9	14.70	11.77	10.26	9.44	7.25	5.66	K8	0.61	0.75	2
56	T 45a	Y00YYY	WTT	15.2	12.38	10.57	9.37	9.24	8.1	6.6	M0	0.45	0.7	3
58	T 46	Y00YYY	CTT	13.1	11.62	9.91	8.96	8.45	6.83	5.20	K8	0.75	0.75	2
61	ISO 237	0000Y0	CTT	16.1	13.75	10.93	9.44	8.62	6.63	4.75	K5.5	1.3	0.9	1
74	T 48	YY0YY0	CTT	14.1	13.07	11.26	10.45	10.04	8.02	6.29	M1	0.15	0.6	10

Table 3—Continued

#	Star	Prop Flag	Class	Photometry						HR Diagram				
				R	i/I	J	H	K	m(6.7)	m(14.3)	SpTy	L_{bol}	Mass	Age
(1)	(2)	(3)	(4)	(5)	(6)	(7)	(8)	(9)	(10)	(11)	(12)	(13)	(14)	(15)
75	Hn 13	0Y00Y0	CTT	16.3	13.95	11.16	10.42	9.91	8.56	7.09	M5.75	0.16	0.08	6
79	Field	17.5	16.06	14.37	13.57	13.23
84	Field	15.5	...	14.40	14.04	13.83
86	Field	20.5	...	16.8:	15.7:	>15.0
88	Field	18.1	...	16.04	15.16	15.0:
91	CHXR 48	YYYY00	WTT	13.4	12.35	10.86	10.08	9.80	8.02	6.29	M2.5	0.25	0.4	3
98	Field	16.0	...	14.55	14.13	14.08
99	Field	15.5	...	14.19	13.66	13.54
100	CHXR 84	0Y0Y00	WTT	16.2	13.97	11.77	11.11	10.78	M5.5	0.082	0.12	1
103	T 50	YY0Y00	CTT	15.4	13.41	10.96	10.18	9.84	M5	0.19	0.2	<1
105	T 51	0Y0Y0Y	WTT	9.9	10.22	9.28	8.52	8.00	K3.5	1.1	1.2	5

Note. — 3. Six character flag indicating the properties of that star from Carpenter et al. (2002): Variable in optical or K; H α emission; Li absorption; X-ray source (prior to the present study); infrared excess; far-infrared source.

4. WTT = weak-lined T Tauri star, CTT = classical T Tauri star, I = imbedded, BD = brown dwarf, AB = Herbig AeBe star.

5-11. R magnitudes from the USNOB-1.0 catalog, i or I magnitudes from the Second DENIS data release or our SAAO I survey, JHK magnitudes from the 2MASS survey, and 6.7- μm and 14.3- μm magnitudes from the ISO survey.

12-15. Properties for cloud members from Luhman (2004).

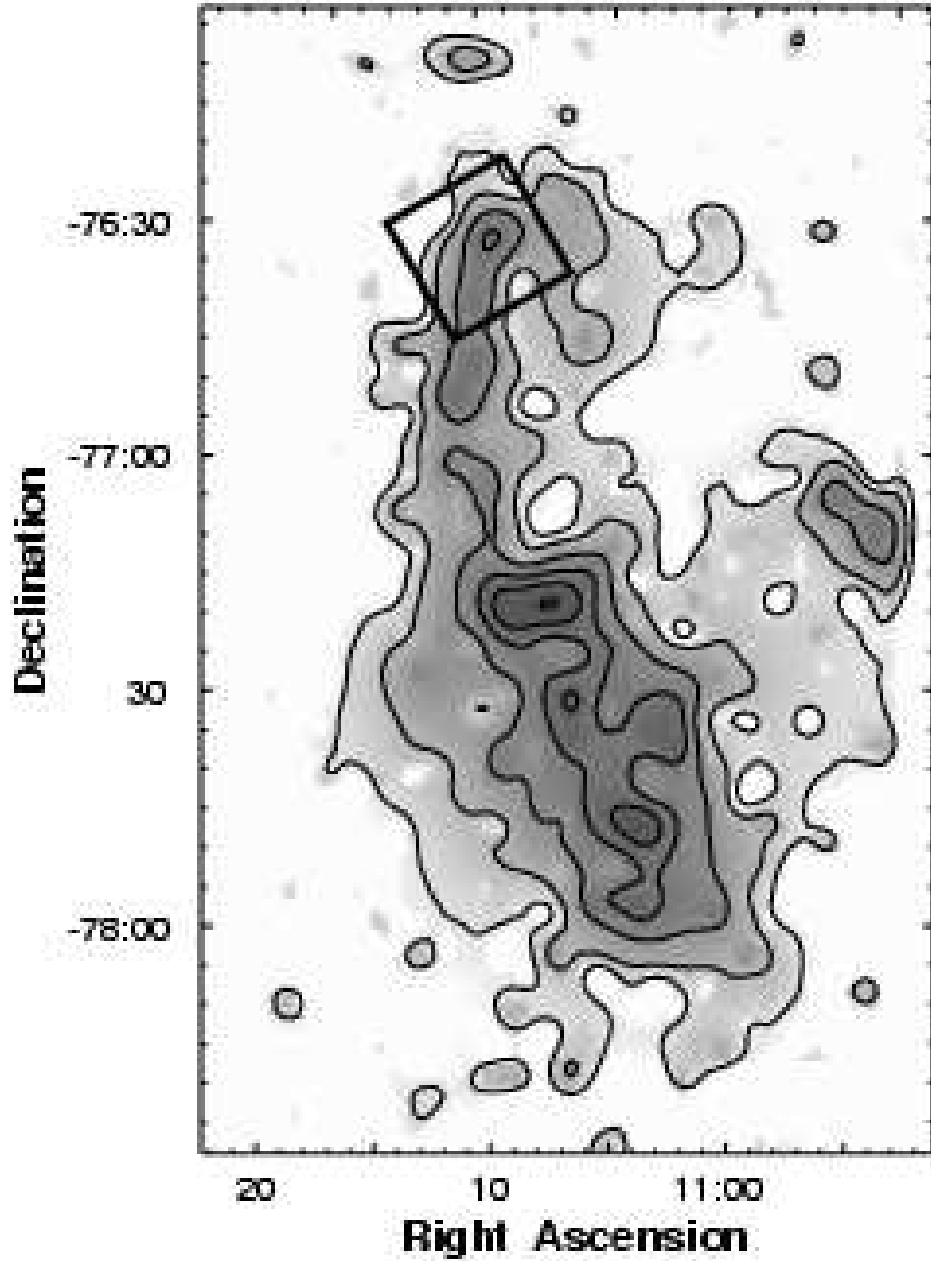


Fig. 1.— Map of the Chamaeleon I cloud showing the *Chandra* ACIS field. The map is in visual magnitudes of absorption derived from *DENIS* star counts with contours at $A_V = 1, 2, 4, 6, 8$ and 10 (Cambresy 1997). The box shows the *Chandra* ACIS field of view.

This image not available in astro-ph version

Fig. 2.— *Chandra* ACIS image of the Cha I North field shown here at reduced resolution ($2''$ pixels). Sources are numbered as in Table 1. Large numbers indicate sources with stellar counterparts (Table 2), while the others are probably extragalactic.

This image not available in astro-ph version

Fig. 3.— Diagram of *Chandra* stellar sources in the Cha I North field. Labeled open circles: Previously known members detected with *Chandra*. Crosses: New *Chandra* sources with stellar counterparts; source #16 (\otimes) is a tentative new cloud member while the others are probably background field stars. The greyscale shows the cloud cores from the *DENIS* absorption map (Figure 1) and the square shows the ACIS field of view.

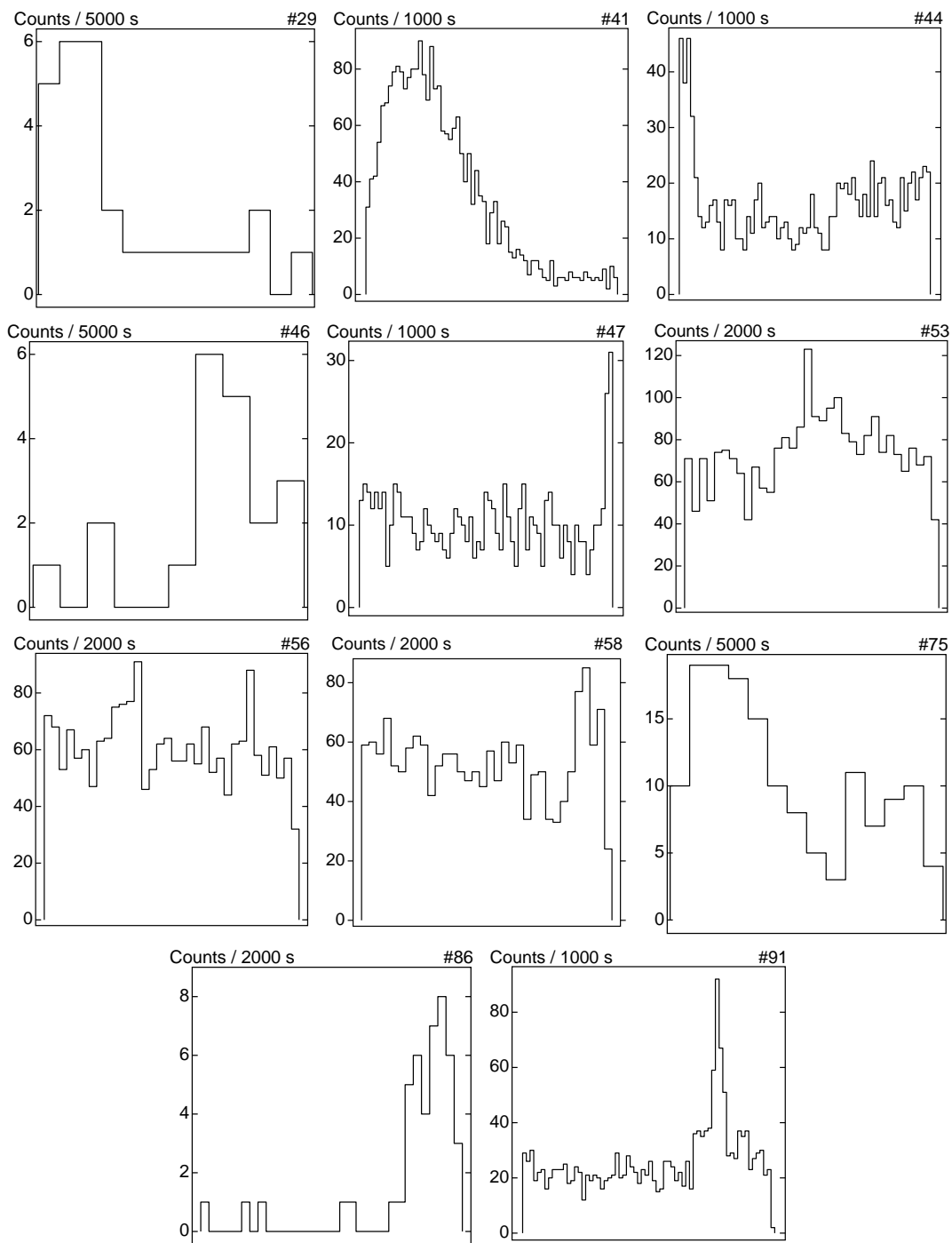


Fig. 4.— *Chandra* ACIS lightcurves of variable X-ray stars in Cha I North: (a) ACIS source #29 = C 1-6; (b) #41 = C 1-25; (c) #44 = T 41 = HD 97300; (d) #46 = ISO 217; (e) #47 = T 42 = HM 23; (f) #53 = T 44 = WW Cha; (g) #56 = T 45a = GK 1; (h) #58 = T 46 = WY Cha; (i) #75 = Hn 13; (j) #86 = background dwarf; (k) #91 = CHXR 48. The abscissa show the photon arrival time from 0 to 66.3 ks. The ordinates show counts arrived in bins ranging from 1000 s to 5000 s, as specified in each panel. No background has been subtracted and standard \sqrt{N} errors apply.

This image not available in astro-ph version

This image not available in astro-ph version

This image not available in astro-ph version

Fig. 5.— Relationships between X-ray luminosity and various stellar properties. The four panels compare the observed 0.5 – 8 keV luminosities $\log L_t$ (units of erg s^{-1}) to: (a) the observed K -band magnitude without correction for absorption or disk contribution, (b) the stellar luminosity $\log L_{bol}$ (units of erg s^{-1}), (c) stellar age (units of Myr), and (d) stellar mass (units of M_\odot). In panels (a-d), filled circles are confirmed cluster members whereas in panel (a) open circles are unrelated X-ray selected field stars. In panel (c), upward arrows indicate cluster members with upper limit ages of 1 Myr.

This image not available in astro-ph version

Fig. 6.— Plot of X-ray luminosities $\log L_t$ and K magnitudes for the complete sample of 27 Chan I North stars (large circles) compared to a sample of 399 X-ray/infrared stars from the Orion Nebula (small dots) with K magnitudes adjusted to match the distance of the Chamaeleon cloud. The shaded band shows the X-ray sensitivity limit of the present observation.

This image not available in astro-ph version

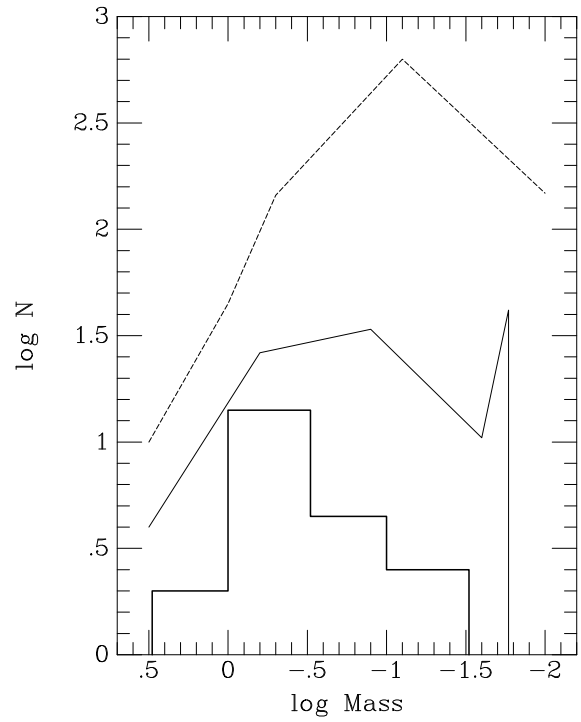


Fig. 7.— The (a) K -band luminosity function and (b) Initial Mass Function of the 27 Cha I North stars (thick histogram) compared to the Orion Nebula Cluster (thin histogram) adjusted for distance. The Orion KLF and IMF are from Muench et al. (2002). The Galactic stellar IMF from (Kroupa 2001) is shown as a dashed line with arbitrary normalization. Chamaeleon star properties are obtained from Table 3.